Borebots: Unlocking Subglacial Lake Access
in the Mars South Polar Layered Deposits
PI: Quinn Morley   Co-I: Tom Bowen

BOREBOTS: UNLOCKING SUBGLACIAL LAKE ACCESS IN THE

MARS SOUTH POLAR LAYERED DEPOSITS

Quinn Morley and Tom Bowen

Planet Enterprises

webinquiries@planet.enterprises

https://borebots.fyi/

CONTENTS

A PRIMER ON THE SOUTH POLAR LAYERED DEPOSITS

The South Polar Layered Deposits (SPLD) is an ancient ice cap, comprised mainly of water ice and dust. It was laid down over millions of years as successive layers of ice and dust, in both annual cycles and obliquity cycles. The thickness of individual layers isn't known to any certainty, but both thin layers and thick layers are visible in images taken from orbit. Generally, the SPLD is water ice with 10% to 15% dust content. This "bulk density" varies by location. For example, some areas may be almost pure water ice, and some may contain up to 25% dust on average (Li et al., 2012; Arthern et al., 2000). The way the dust content in the ice varies from layer to layer is unknown, but it is thought that layers can range from <1% dust to 50% dust. The multiple types of layering may represent the complex way the annual, precession, and obliquity cycles interact (Smith et al., 2020, section 1.2).

During rare and unique conditions within the obliquity cycles, large quantities of CO_2 ice can be trapped by a water ice layer that gets deposited on top of it, which can be seen in the "Reflectance-Free Zone" (RFZ_3) shown in Figure 1 (Phillips et al., 2011). However, there is no evidence for large quantities of buried CO_2 ice near the area being considered in this study (Putzig et al., 2011). Generally, water ice is deposited slowly enough that CO_2 capturing like this is rare. Said another way, CO_2 can escape from under thin layers of water ice (this is called cryptic terrain, and can happen annually), but not thick layers. It is only trapped permanently when buried under a thick, nonporous layer at a sufficiently fast rate (Manning et al., 2019).
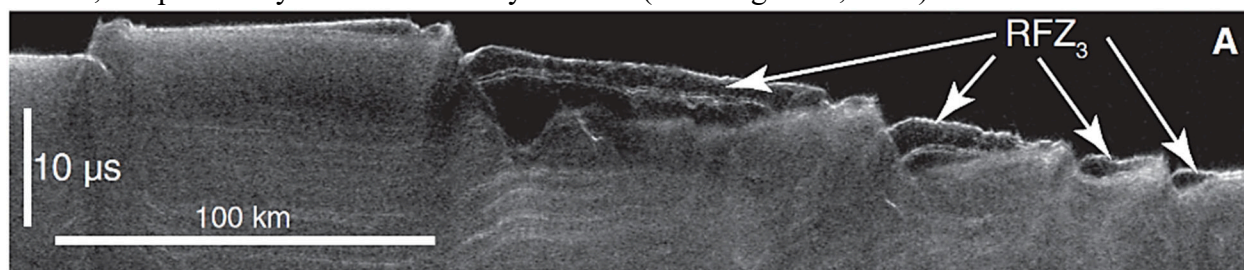

Figure 1, a SHARAD radargram showing RFZ_3 (Phillips, et. al, 2011, Fig. 1A).

When water ice forms on the surface of the cap (either as snow, or frost) it appears to densify differently than snow does on Earth; however, we have to extrapolate this from what we can see and sense from orbit. It is believed that vapor exchange with the thin and cold atmosphere helps the old snow (firn) become very dense after it is buried by only a few meters of additional snow/frost (Arthern et al., 2000). On Earth, this can take hundreds of meters of depth to occur, and is driven by compaction due to gravity. The exact densification process at the poles is not known. The important takeaway here is that there doesn't appear to be a top "firn" layer in the SPLD (Clifford et al., 2000; Smith et al., 2020; Vasavada et al., 2000). This is good news for those who wish to drill into the formation. It is also worth noting that the age of an ice layer at a certain depth is much older on Mars when compared to the same depth on Earth. This means that ice on Mars densifies much sooner if you are measuring depth, but much slower if you are measuring time.

The SPLD seems to be in a state of very slow decay, either from drainage winds called katabatic winds – which also occur on Earth – slowly eroding the surface, or from the ice vaporizing (called sublimation), leaving behind a layer of dust that gets cemented by ice in

following seasons. It is likely that a combination of both processes occurs. For these reasons, it is expected that a lander would touch down on a thin layer of loose dust, under which would be ice-cemented dust that would be hard like rock. This kind of a layer is called a "sublimation lag layer" (Byrne, 2009). We don't know the specifics of this layer, although it may be up to 100 meters thick. We have reason to believe that it is at least 30 meters and less than 45 meters, but this is simply an early hypothesis to explain a "fog" effect seen in radar returns from the SHARAD Ground Penetrating Radar (GPR) instrument of the Mars Reconnaissance Orbiter (Whitten & Campbell, 2018; section 4.2, para. 2). Ground-based GPR is already flight-proven (the Perseverance rover is fitted with a GPR instrument called RIMFAX, see Farley et al., 2020); so, we should be able to estimate the lag layer thickness much more accurately after touching down.

In 2018 the planetary science community was shocked by the announced detection of what could be a liquid water lake under the SPLD, in an area centered on 81° South, 193° East (Figure 2). This area is now commonly referred to as the "high-reflectance area," and is about 1.5 kilometers under the ice (Orosei et al., 2018a, 2018b). The team of Italian researchers used data collected by the MARSIS instrument on the European Space Agency (ESA) Mars Express orbiter, and presented a very convincing and thorough case for their determination. However, due to the extraordinary nature of the claim, the issue remains hotly contested (Sori & Bramson, 2019; Lauro et al., 2019; Lalich et al., 2021). It appears as though the most likely alternative hypothesis is some kind of hydrated sediment layer under the SPLD, like frozen clay or mud (Bierson et al., 2021; Smith et al., 2021).
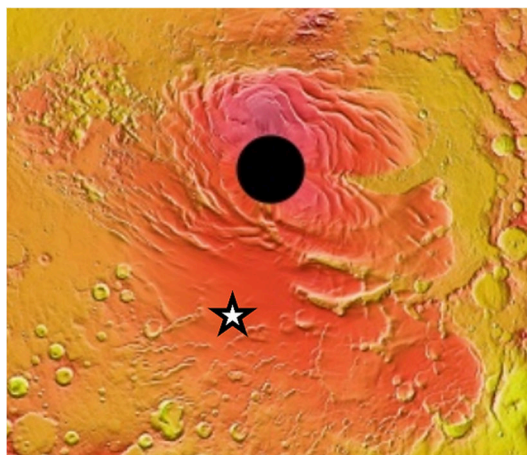

Figure 2. View of the SPLD with elevation relief. The High-Reflectance Area from Orosei, et al. (2018) at 81°S, 193°E indicated with a star. NASA/JPL/University of Arizona (uahirise.org)

Although the poles are very different, we anticipate that a mission to the North Polar Layered Deposits (NPLD) would pose the same challenges and level-of-difficulty as the SPLD. Specific drilling challenges may apply more to one pole or another; however, overall feasibility of deep drilling in a Martian polar environment is shared between the two geographic locations. For this reason, SPLD and NPLD deep drilling missions are treated as interchangeable in this report.
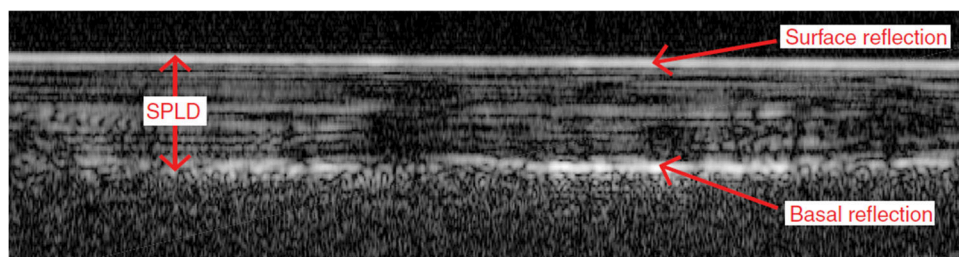

Figure 3, a MARSIS radargram showing the High-Reflectance Area at the base of the SPLD. From Orosei, et al. 2018a (Figure 2A, p. 3).

MISSION CONCEPT & BOREBOTS DRILLING ARCHITECTURE

Mission Concept

The mission concept centers around deep drilling into the SPLD, and extracting ice cores. As a primary mission goal, it was decided that 50 meters is the most prudent numerical target and that it should be achievable in 90 days. However, to lend a more logical basis to the selection of the primary goal, we can say the depth should be enough to make it through the sublimation lag layer (plus any transition layers) and into the bulk of the formation itself. Once an ice core is retrieved from below the lag layer, the primary mission will be successful. Unfortunately, today we do not know the thickness of this lag layer, but it is likely to be somewhere between 30 and 45 meters thick. Although coincidental, this reasoning supports the primary target depth of 50 meters in this mission context. Regarding the length of the mission, in order to mitigate the risk from unexpected challenges slowing the drilling operation (which are likely), the landing should be timed such that a full Martian southern summer is available to complete the primary mission. If planned for mid-spring to mid-autumn, this could equate to roughly one Earth year, staving off the risk associated with the long and unforgiving polar winter affecting the primary mission.

The science return from this primary mission goal would be virtually unrivaled in Mars exploration, if successful. Just centimeters below the surface there may be frozen life, alive or dead (McKay & Stoker, 1989, p. 16-17). This offers a plausible astrobiology context for the primary mission goal. Deeper layers may hold a record of life-bearing layers that existed in the past. Astrobiology aside, merely drilling into the SPLD and visually imaging the borehole would dramatically change our knowledge of the climate and geophysical history of Mars on a time scale of millions of years. Going beyond simple imaging, the addition of downhole science instruments and surface sample processing (life detection, precision gas analysis, etc.) could create a potentially robust science return, enabling decades of discoveries that would indisputably change our understanding of Mars.

The extended mission goal is to drill through the entirety of the formation, using a triaged approach to science activities and sample processing. As depth increases, the secrets of Mars' obliquity and climate cycles will be revealed. Ice conductivity & density data can help scientists better understand orbital remote sensing data, allowing them to predict what lies ahead for the drilling operation as we begin to understand the stratigraphy better. If landing near 81° South, 193° East, the basal unit may contain a liquid water lake or frozen hydrated sediments at a depth of 1.5 kilometers, as previously discussed. In a follow-on study examining the high-reflectance area, Lauro et al. hypothesized that a form of ancient super-cooled brine may be present under the ice, stable for millions of years, which could contain oxygen. Lauro et. al concluded:

> "The water bodies at the base of the SPLD therefore represent areas of potential astrobiology interest and planetary protection concern, and future missions to Mars should target this region to acquire experimental data in relation to the basal hydrologic system its chemistry, and traces of astrobiological activity" (2021).

The basal unit and surmounting ice have also witnessed eras of the Martian past, and are certain to contain records of these periods in the ice. In 2005, Smith and McKay recommended drilling in this region, concluding:

> "At depths of ~1000 m, the effect of the obliquity cycle is dampened and permafrost at this depth would be unaltered over geological time. Biological material, rather than a mineralized fossil, is needed if we are to determine if Martian life represents a second independent genesis. Deep drilling on robotic or human missions could be focused on obtaining this material in ways that do not contaminate the Martian subsurface…" (p. 6).

On the other side of the pole, an ancient formation called the Dorsa Argentea Formation (DAF) covers a much larger area, rivaling or exceeding the age of deposits discussed by Smith and McKay (Head & Pratt, 2001). However, it appears that the DAF extends under the SPLD (Whitten et al., 2020, section 4). The DAF and the area studied by Smith and McKay may both be remnants of an older ice cap, which is simply in varying states of decay. If this is the case, the younger SPLD materials may be protecting material that witnessed the climate events of 3.5 billion years ago. Only deep drilling can reveal the truth.

The extended mission goal is likely to take 5-10 years, with a duration less than 3-4 years being unlikely. Therefore, two or more Martian polar winters are expected. It is impossible to consider this mission low-risk; however, each meter descended is extremely valuable (for the reasons outlined above), therefore, the rewards increase in proportion to the risk in the extended mission phase.

An auxiliary extended mission goal would be to drill additional boreholes at locations identified during an exploration phase, which could occur during the first weeks after landing. Exploration by the rover, by scout helicopter(s), or by intense orbital imaging could identify these locations of interest. The first drill site would occur at the most promising location; however, if the drilling operation is forced to abandon the borehole, a new borehole could be started at an additional location nearby instead of attempting to salvage the depth attained at the first drill site. It is the goal of this investigative team to give mission planners and scientists the utmost flexibility while contemplating these decisions. Therefore, the drilling architecture outlined in the following sections of this report provide several redundant operating modes, and represents a robust capability that could start several new boreholes throughout the mission (even after a catastrophic loss of downhole equipment); or could enable branching of the borehole above a failure location by using advanced autonomous drilling techniques so drilling can continue. In all cases the challenges associated with the Martian polar environment are kept in mind. Deep drilling in to the SPLD is used as the mission context whenever possible in this report, in order to provide a consistent and fair analysis.
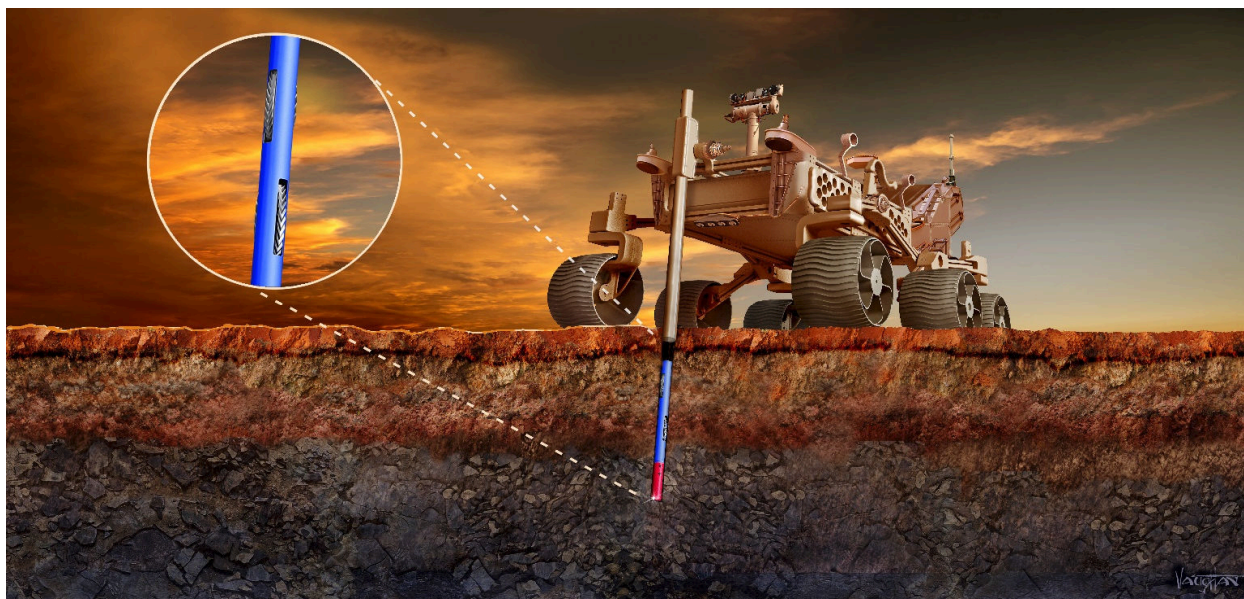
Figure 4: A borebot being deployed from a tube on a rover. James Vaughan Illustration.

Borebots Deep Drilling Architecture

Self-driving drilling robots that are approximately one meter in length (borebots) perform deep drilling activities autonomously from a large rover, very close in capability to the Mars 2020 / Perseverance Rover (as described in Farley et al., 2020), shown in our concept art (Figure 4) at the top of this page. Ideally, the NASA Jet Propulsion Laboratory (JPL) would be able to produce a twin of Perseverance that would require only slight modification to accommodate the borebots architecture. Notable modifications include the addition of a three Degree of Freedom (DoF) deployment tube mechanism opposite the existing robot arm (shown in Figure 5), and the replacement of the MOXIE technology demonstration instrument with a science payload. Other requirements include adding borebot servicing capabilities (cleaning, charging, assembling, etc.), and a reduction in turret science payload to make room for a capable tube-grasping end effector. The rover and drill heads shall be treated as strawmen here, with Perseverance used as an example. The system can work with any sufficiently-equipped lander or mobility platform, and with a variety of drill head designs.
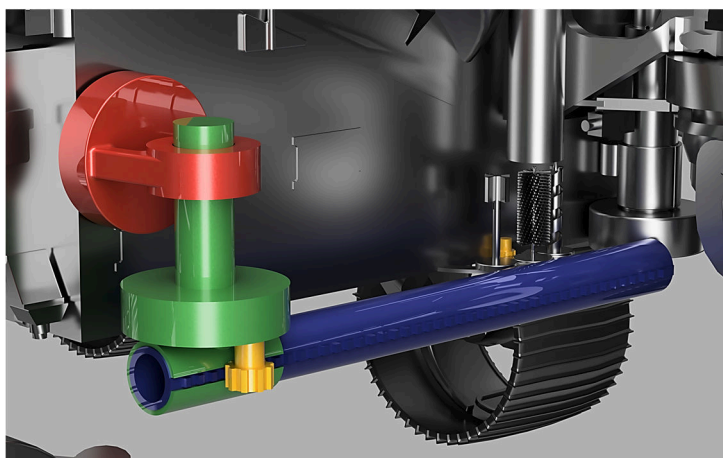

Figure 5: A deployment tube with 3 Degrees of Freedom.

When a suitable location is found to begin the drilling operation, the initial drilling sequence starts with the movement of the deployment tube into the drilling position (Figure 6). Ideally, a borebot is flown to Mars pre-assembled and loaded in the deployment tube. This allows for drilling several meters and taking dozens of ice cores even if the robot arm were to fail catastrophically upon deployment. The pre-loaded borebot
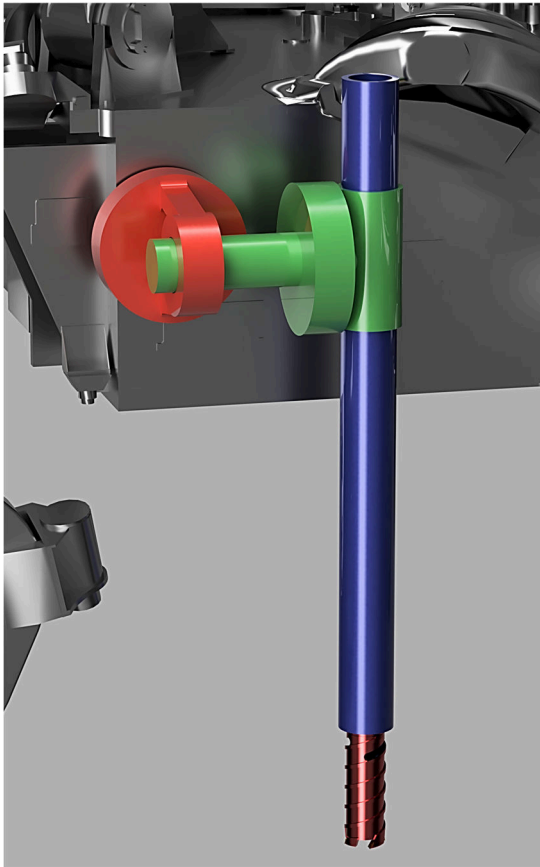
drives down the tube and begins the automated drilling procedure, taking a ~40 mm by 150 mm core. While the automated drilling process is being carried out by the first borebot, a second drill head is retrieved from a storage location and loaded into the assembly station (Figure 7), and a second borebot is retrieved from storage and mated to it. This second borebot is now standing by for deployment (waiting for its turn). When the first borebot completes its drilling cycle, it drives up the deployment tube and waits for the tube to move to the re-coring station (Figure 8). It is worth noting that borebots can either be pre-assembled, or assembled via an automated workflow *in-situ*. Spacecraft mass, volume, and budget considerations (along with the desired drilling depth) are the primary driver in this decision.

The automated re-coring process is carried out next. Either the borebot can provide the rotation for re-coring, or the re-coring station on the rover can have a motor built-in. The re-coring station uses the same drill bits and samples tubes that Perseverance uses for rock coring (Moeller et al., 2021). During re-coring,
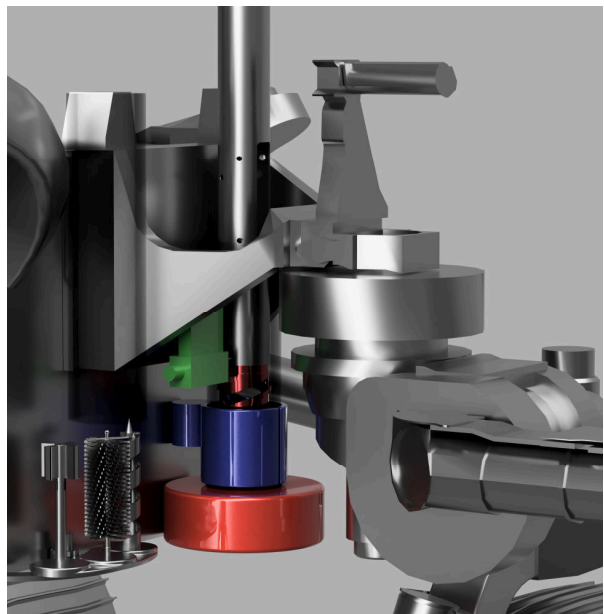

Figure 6: Deployment tube in drilling position.

the chips and dust that are created are blown into a pneumatic sample handling system, which can route the samples to instruments or dump them overboard if not needed (this pneumatic collection

is similar to the system used on the Dragonfly hexacopter, see Zacny et al., 2019). Since these chips come from the center of the ice core, they are much purer than the chips created by the borebot when originally taking the core. After re-coring, the drill bit and sample tube are moved from the re-coring station to the Adaptive Caching Assembly (ACA) bit carousel; see Figure 10 (Novak et al., 2019). The drill bit will be swapped for a new or sanitized one, and will be fitted with a new or sanitized sample tube.

The deployment tube moves back to the drilling position, allowing the borebot to drive *up* the tube to offer itself to the robot arm. This allows the robot arm to remove it from the tube and move it to the cleaning station (shown next to the assembly station in Figure 8). In the cleaning

Figure 7: Assembly station integrated into the mounting bracket for Perseverance's 5-DoF robot arm.

station the remaining debris are removed. Once placed in the cleaning station, the next borebot (that has been waiting on standby) is moved to the deployment tube by the robot arm, and the cycle begins again. Battery charging can be accomplished during a borebot's stay in either the cleaning station or the assembly station.

Notably, the order of operations for the re-coring process will change during the extended mission (depth greater than 50 meters) phase: the first borebot (when surfacing, after drilling) would instead be placed in a staging area (likely the cleaning station, next to the assembly station) while the next borebot is deployed via the tube. Then, the first borebot (that still needs re-coring) could be placed back in the deployment tube so re-coring can occur while the longer driving/drilling cycle inherent to deep drilling is occurring down the hole.

This compact and simultaneous mode of autonomous operation would be impractical with any other drilling architecture. To provide flexibility to mission planners, the cleaning station must be capable of cleaning the drill head completely (even if re-coring is skipped), and it should be tied-in to the pneumatic sample handling system. This way, if a core is only desired every few meters, time and wear-and-tear could be saved by skipping re-coring. Samples (chips / debris from the drill head cleaning process) can be routed to instruments pneumatically if desired.
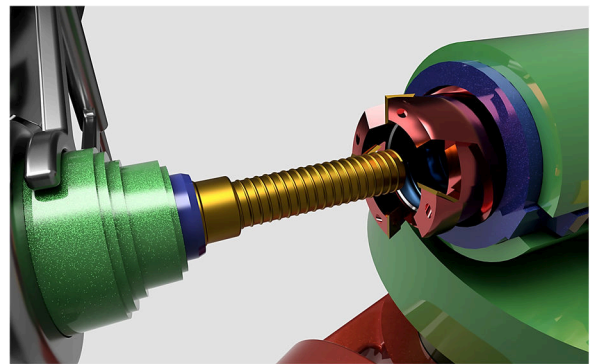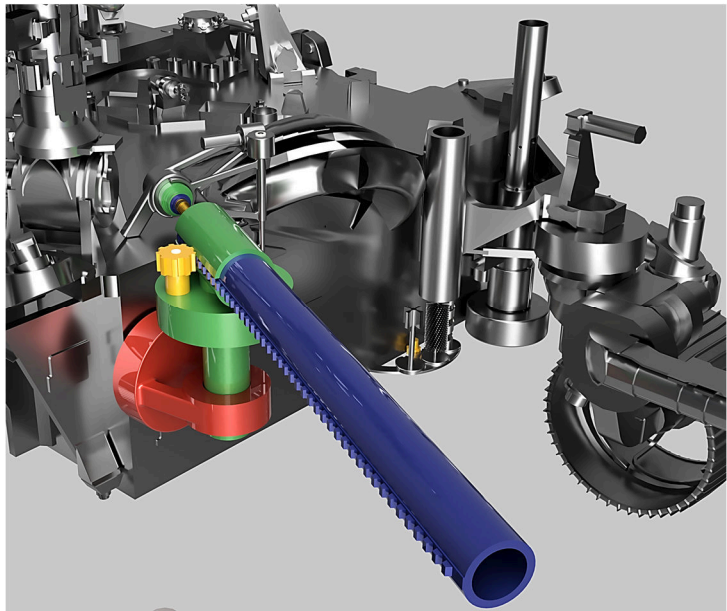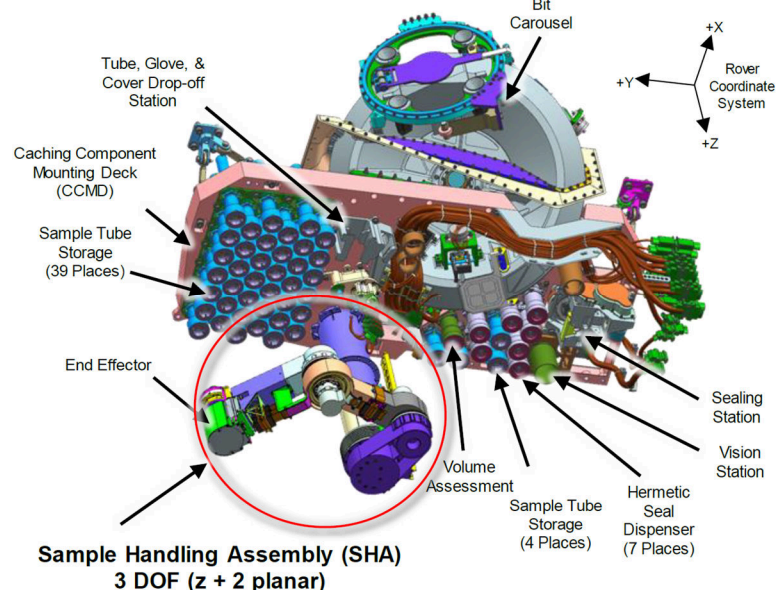

Figure 8, 9, & 10 (top to bottom): Deployment tube offering a borebot to the re-coring station, re-coring close-up showing ACA drill bit, and an overview of the Perseverance ACA from Novak et al. (2019, fig. 3).

The drilling, re-coring, cleaning, and staging cycle continues for as long as is necessary. Eight to twelve borebots can be brought to offer a measure of redundancy, or to spread out the component wear-and-tear among a greater number of robots. Having the option to distribute the drilling workload is the key advantage to the borebots deep drilling architecture, and as we will see in the Alternate Borebots Architectures section, is easily adapted to other mission classes.

Borebots Technical Discussion

On Earth, deep drilling requires a massive infrastructure (most of it at the surface) and relies heavily on manpower and fuel-burning generators. There is always some physical link with the surface, either a tether or steel drill pipes (Bar-Cohen & Zacny, 2009, pp. 320-328). One of the leading deep drilling systems designed for use on Mars is shown in Figure 11 at the right. Known as Auto-Gopher 2, it belongs to the "Planetary Deep Drill" family of drills developed by Honeybee Robotics (Zacny, 2016), with part of the funding provided by the Planetary Society (Davis, 2018). Along with its cousin WATSON (Eshelman et al., 2019; Malaska et al., 2020), these drills represent the state of the art for 100-meter-class extraterrestrial deep drills. The high degree of miniaturization and automation mean far less surface infrastructure than most systems designed for use on Earth. However, the current versions of these drills rely on towers over three meters tall, large winches, generators for power, and human intervention to remove cuttings or cores from the drill head.

At the heart of the borebot concept is the idea to replace the tether with some kind of driving apparatus. A large spool of cable (the tether) can be seen at the base of the drill rig in Figure 11, which is an absolutely critical component of a wireline drilling system – a failure of the winch or

Figure 11: Auto-Gopher 2 deep drill during testing at the Fish Creek gypsum deposit in California (Davis, 2018). The drill and rig are both over 3 m tall. A generator can be seen in the background.

tether is a failure of the mission. These components are so large and heavy that it may be impossible to carry a spare. Struggling with the ramifications of this problem is what kindled the desire for a self-driving system with a high level of redundancy (multiple units and spare parts). Thus, the borebots concept was born.

A suitable drive system was first hacked together in 2018 (Figure 13; video: https://git.io/JBbJ1), during night and weekend fabrication and experiment sessions by the PI. The first functioning mockup drive system was envisioned to be "squish-fit" into the borehole, maintaining pressure against the borehole wall by using the Hooke's law behavior of the flexible components. To accentuate this effect, the drivetrain was staggered, so the tank tracks could act like rubber bands, and would spend most of their time under tension. Tension increases as the components pushed against each other. Herringbone gears were used to provide intrinsic stability and self-centering of the belt and gear system. This allows for the addition of "idler" gears that can free-float inside the tracks, providing more "squish" to evenly distribute the traction forces on the borehole wall. The gear geometry was based on a design by Emmett Lalish and was published on

Figure 12 (left): A borebot is shown in its natural habitat, and with two pairs of tracks. As shown, the borebot has just finished the deployment sequence by driving out of the tube and to the bottom of the borehole to being drilling.
Figure 13 (center): Mark 1 drive system mockup with floating idler gears to intensify pressure at borehole interface.
Figure 14 (right): Schematic of the drive system, with gears shown doubling as "tank tracks." Idlers omitted.
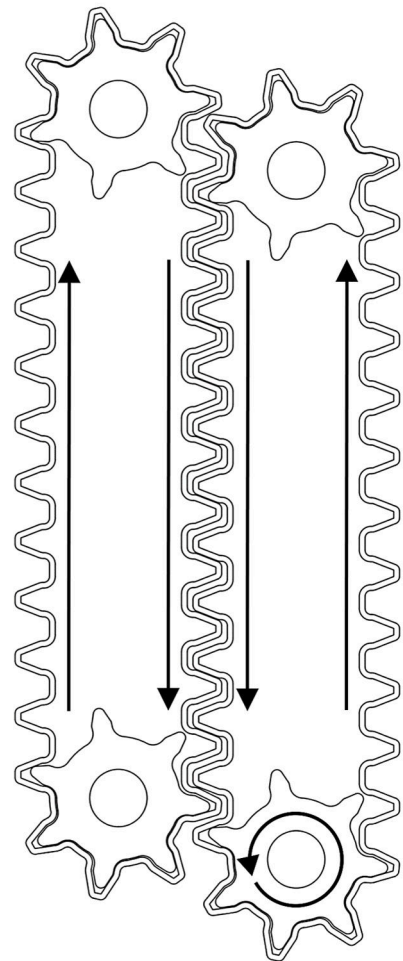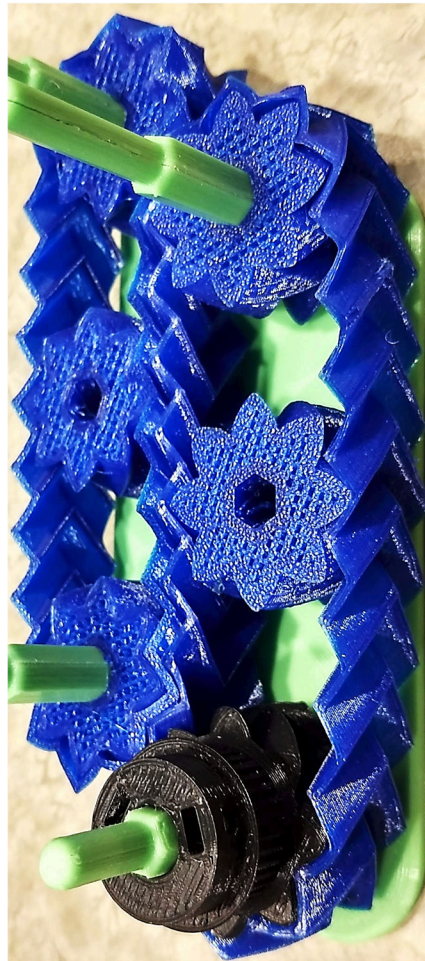
Thingiverse.com to respect the open-source license (Morley, 2019; Lalish, 2013). The potential for one of the idlers to become misaligned and shift towards one of the other gears does exist. Therefore, floating idlers may not be in future designs; however, it remains a convenient layout for testing. A borehole size of 64 mm was chosen, as it matches the original Planetary Deep Drill diameter and represents the practical lower size limit for a robust mechanical system of this type.

A consequence of the squish-fit design is the "linking" of the tracks, meaning that drive power only needs to be applied to one track, and the power is transmitted to the other track as through a pair of gears (Figure 14). This has advantages with respect to miniaturization and robustness, but also has disadvantages. Some positives of the linked system are that only one motor is required for each pair of tracks, more space is available for each mechanical component (because they nest into each other), small bits of ice and rock can pass through the middle of the system, and the presence of a "mechanical fuse" (the tracks can skip past each other and then resume normal operation; this can also be thought of as a safety clutch). The disadvantages of the linked system are a lack of independent track control, lack of pressure control (normal force against the borehole is controlled by the Hooke's law behavior of components and is not adjustable on the fly), and greater mechanical energy waste due to friction. The force against the borehole is also kept relatively high due to the "preload" tension in the system, which is a prerequisite to enjoying the benefits. It may be possible to mitigate some of these disadvantages by creating a sliding mechanism for one of the tracks, to adjust the stagger distance and therefore the pressure on other components (preload tension) and the borehole. The "Mark 3" prototypes have been developed without the staggered approach, although early work shows that the self-tensioning effect from the staggered components is missing, and belt tension becomes a critical design factor (and one that may need to be controlled in order to guarantee trouble-free operation over the life of the mission).

In order to continue the discussion about the flexible gear drivetrain, it is important to understand the method via which the 3D printed gears were made. In the prototype stage, the inventor has a high degree of control over the compliance of the printed components using a few simple techniques. In more advanced design stages, analytical methods can be used to define an internal structure that strictly
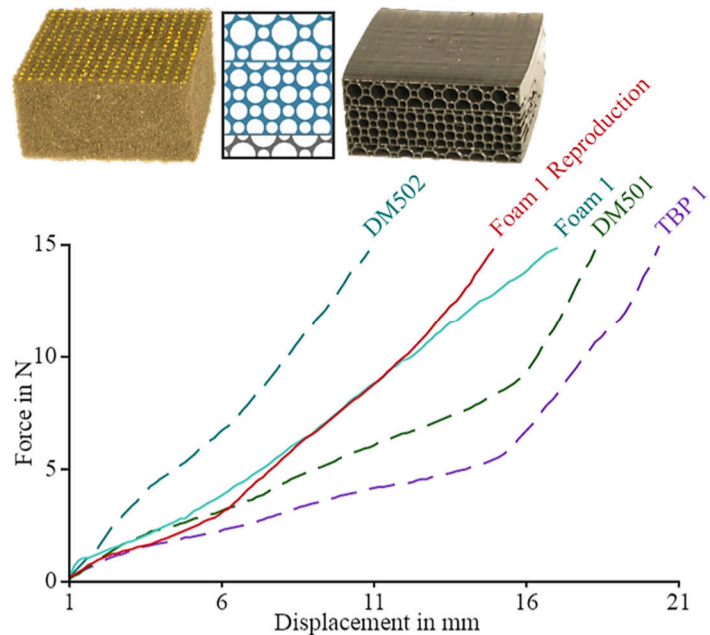

Figure 15: Figure 10 from Bickel et al., 2010.
DM502, DM501, and TBP 1 are 3D printing materials that are being combined (stacked) to reproduce Foam 1. Designers have complete control of the "cell" geometry. The slicer creates toolpaths such that the part is created 100% solid, creating a machine program capable of producing the cell structure geometry in a physical part exactly as it was input.

controls the way the gears deform when compressed. This can enable finite-element simulation of component performance, and offer strict configuration control which can allow for physical testing and statistical analysis. Using an analytical approach to achieving the correct pressure on the borehole wall (via the control over the component properties) may also allow for the selection of existing materials that have less-specific fabrication requirements, decreasing cost and possibly increasing component reliability due to a more isotropic material response.

Figure 16: Each color is a "family" of unit cells; 6 examples of each family are shown. The 3D unit cells build on the work of Bickel et al., allowing control of elasticity as a fn. of location (Schumacher et al., 2015, figure 13).
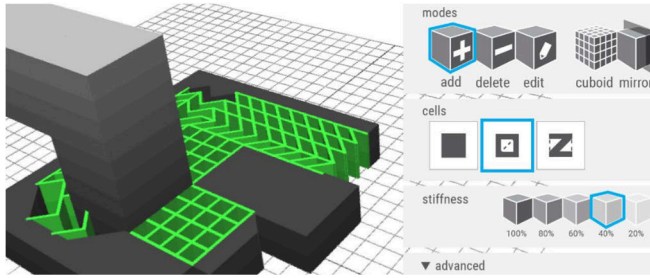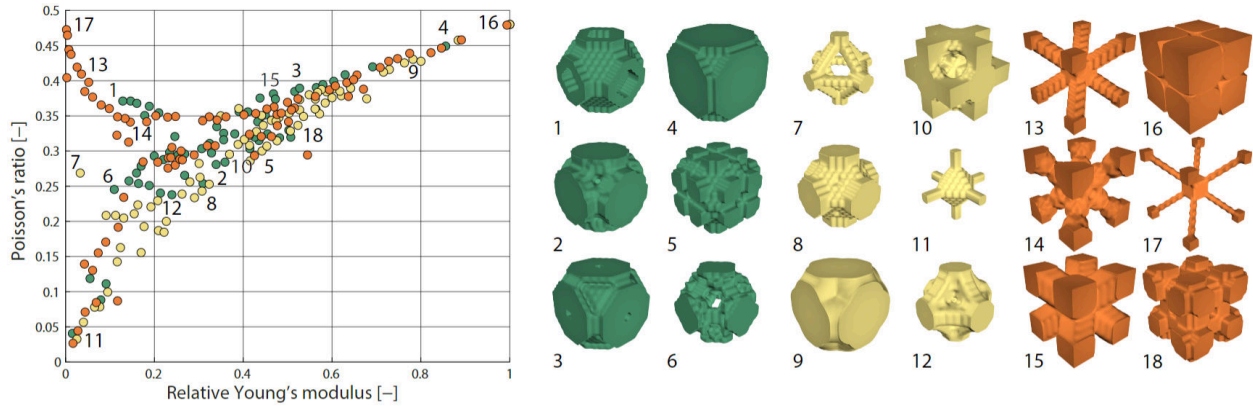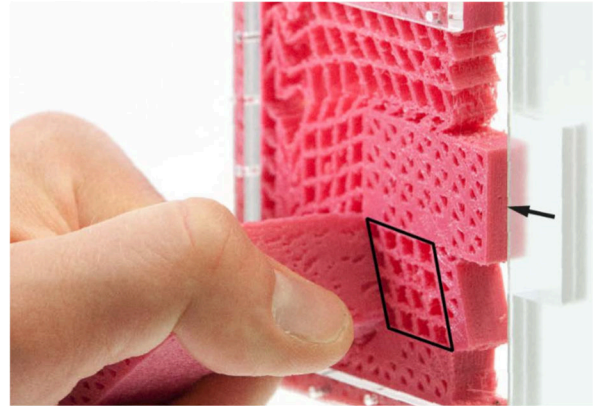

Figure 17 (above): Screenshot from the editor, available at https://jfrohnhofen.github.io/metamaterial-mechanisms/
Figure 18 (right): A metamaterial mechanism door handle.
Figures from Ion et al., 2016, Fig. 1C and 1B, respectively.

In the context of additive manufacturing (3D printing), the design of materials with a specific deformation behavior is discussed thoroughly in Bickel et al. (2010), with an example shown in Figure 15. Continuing this line of thinking, Schumacher et al. present a technique for controlling the elastic behavior of a material as a function of location within the component volume (2015), see Figure 16. A class of materials called "metamaterial machines" was discussed by Ion et al., and an application was released that allows the general public to design machines composed only of their shear-cell design elements, which is then able to be printed as one complete unit (2016). An example metamaterial mechanism can be seen in Figure 18, and a screenshot from the user-interface of the application can be seen in Figure 17. These works represent methods that can be applied carefully during the design phase to achieve a predictable result.

During the prototype phase, instead of the employing the above methods with their up-front design commitments, a family of techniques known as "slicing tricks" was used to generate geometry that could then be printed and tested. A "slicer" is an automatic Computer-Aided Manufacturing (CAM) software tool that creates lines of code representing discrete vertical increments of a part (or "slices"), which are compiled into a machine program and subsequently used to create a physical part via 3D printing. Since each gear is relatively small (and therefore, prints quickly), an iterative approach was used until the elasticity of the gear was acceptable. Although slicing tricks exist as a form of tribal knowledge within the 3D printing community, it is difficult to find literary references for these techniques. Generally, the idea is to leverage a shortcoming of the technology *to the advantage of the designer or operator*. The first example of effectively using slicer settings to affect the elasticity of a printed object may have been the "Recreus Sneakers" line of DIY footwear, released by the inventor of one of the first widely available flexible filaments, Filaflex (Garcia, 2013, 2014). However, a mention
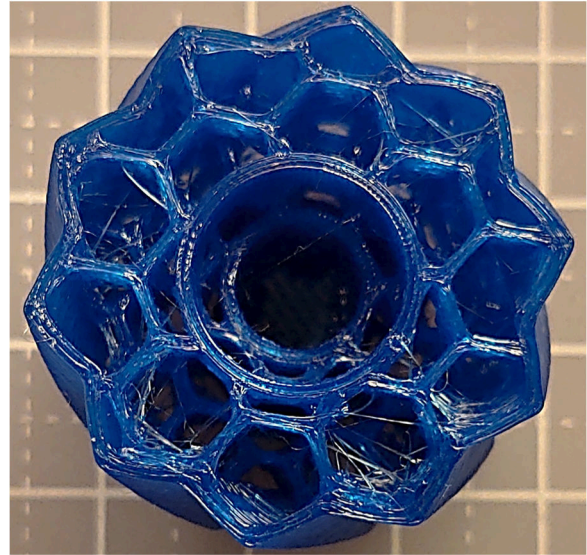
Figure 19: honeycomb fill with no top/bottom layers.

of using property modifiers to force the slicer software to achieve a variable elasticity was mentioned by Dr. Adrian Bowyer, the creator of the first Replicating Rapid Prototyper (RepRap) 3D printer, in a 2011 forum post (Hodgson, 2012, Pg. 1766). Both approaches leverage the fact that 3D printed parts are often fabricated with a "sparse infill" pattern, designed to produce a structure that can quickly take up space during fabrication. Infill plays a minor structural role in most applications, primarily resisting buckling loads, but occasionally supporting high compression loads (Hermann, 2018; Sanladerer & Hermann, 2019). The largest advantage of sparse infill is that it supports the horizontal layers that will be printed later, which makes the fabrication process smoother and of a higher quality.

When considered in the context of flexible materials, the overall part density (and thus, the infill) controls the bulk elasticity of the flexible component to a high degree. One other technique (which likely predates any online discussion or published literature) is to "turn off" the top and bottom solid layers for the part, allowing the infill pattern to have a greater degree of control of elasticity (this can be seen in Figure 19). These techniques were employed by the PI to give the prototype gears less elasticity and more resiliency in the center of the gear, and more elasticity towards the sides. This allows the gear to conform to the radius of the borehole while creating less wasted energy. If a rock is ingested into the track system, the sides of the gear can flex with less force (but contain pockets for the bearings, limiting total deformation); while the center section is more resilient, but offers slightly more available deflection to pass objects through. Moving the bearings from the gears to the Borebot housing may allow for the easier passing of stones; however, when the bearings are placed in the gears, the prototypes are much easier to assemble.

The parameters for slicing the gears used in the Mark 3 drivetrain can be seen in Table 1, while Figure 20 & 21 show the result. NinjaTek Cheetah (Shore 95A) filament was used in all cases. These gears can be printed individually, or in multiples printed simultaneously with the belts (ring gears). The resulting elastic properties of the gear allow it to conform to the borehole (here, a 64 mm ID acrylic tube), as seen in Figure 23 & Figure 24, shows the same for the gear with a belt installed. The gears and belts pictured were generated with a 60° pressure angle, which seems to allow for smoother operation. All pr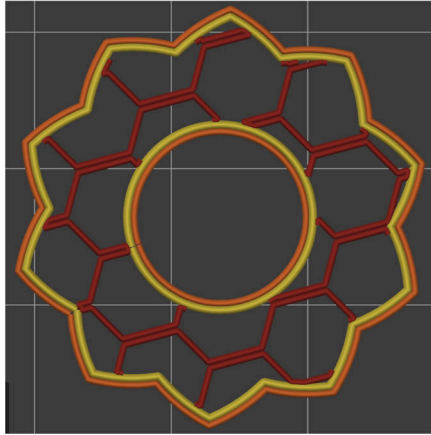e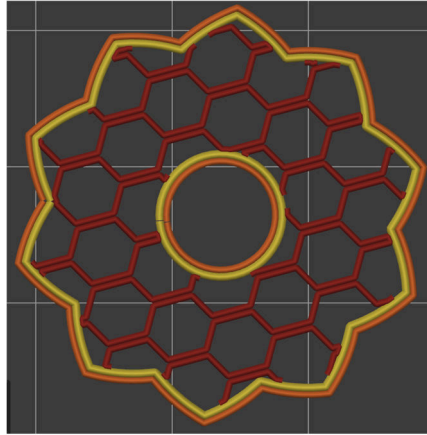vious prototypes were created with a 45° pressure angle, which exhibited a pronounced "clicking" motion as the rolling resistance oscillated with the passing of the gear teeth. Elasticity affects this clicking behavior, but not as much as the pressure angle and the overall pressure in the system. Greater pressure angles may lower rolling resistance further, and both pressure angle and elastic properties are good parameters for optimization (at a 90-degree pressure angle, the gear belt turns into a standard flat belt).

Figure 20: 14% honeycomb infill

Figure 21: 20% honeycomb infill

One problem with optimizing the pressure angle parameter (in the context of stuffing belts and gears into a tube), when the pressure angle is changed, so must be the diameter of every component. This is compounded by each pressure angle / elasticity combination "meshing" (and flexing in response to meshing) in different and subtle ways. For these reasons, the iterative design approach will need to be continued and the diameters that work best will need to be tabulated. This will allow analyses as described earlier in this section to generate geometries which yield the desired elastic properties, but that rely on the tabulated diameters from the iterative design process. From there, more iterations may be required to balance rolling resistance and the force against the borehole wall. The prototype phase of drivetrain development should be continued until the Weight on Bit (WOB) requirements are finalized to mitigate the potential for late-stage redesign of the drive system, by evolving both the drilling requirements and drive system at the same time.

Table 1 - Gear Print Settings - PrusaSlicer 2.3.1	
External perimeters extrusion width	0.50 mm
Perimeters extrusion width	0.60 mm
Infill extrusion width	0.50 mm
Layer height	0.2 mm
Nozzle diameter	0.4 mm
Number of perimeters	2
Number of bottom solid layers	0
Number of top solid layers	0
Infill density	14%
Infill density modifier (middle 11 mm)	20%
Infill/perimeter overlap	30%
Infill pattern	honeycomb
Speed (all print moves)	30 mm/s
Accelerations (all print moves)	250 mm/s^2

Alternatively, components generated with ideal elastic properties could be modified by only a scale factor to compensate for late-stage WOB requirement changes. Another option may be to build-in some form of adjustment for the track system, so the gears can be forced against the wall to increase pressure on the fly (this is discussed in more detail later in this section). This could also be part of a steering mechanism, but could add its own cost and complexity.

Although these tricks are difficult to describe and get an intuitive understanding for, they can be done in practice in a matter of seconds. As briefly mentioned earlier, the first prototype drivetrains (hereafter called Mark 1 and Mark 2) were in fact made entirely from a publicly shared, customizable 3D model called the Gear Bearing (Figure 22) by Thingiverse user Emmett Lalish (2013). Careful readers may have noticed the hexagonal hole in the gears shown in Figure 13. These gears are multiples of the sun gear generated by the Gear Bearing customizable model. The Mark 2 drivetrain replaced the hexagonal hole with round holes in a post-processing step, and eventually moved the bearings to counterbores, in what could best be described as the Mark 2B.
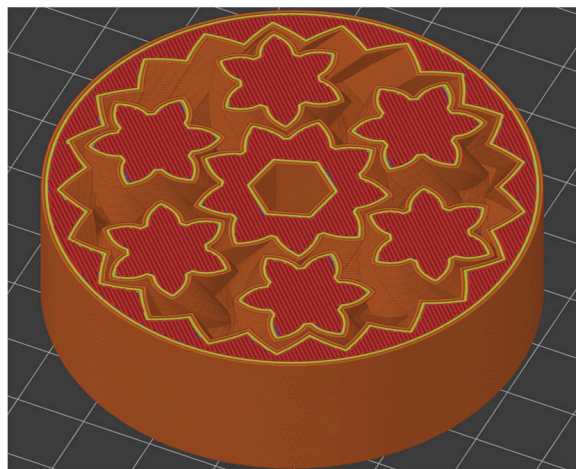

Figure 22: The Gear Bearing sliced normally, as the designer intended. Note the hex hole in the sun gear. The design code for this model was customized to generate the Mark 1 & 2 drivetrain components.

As if this process didn't seem mystical enough to the uninitiated already, the gear-belts for the Mark 1 and Mark 2 prototypes *are the ring gears from the Gear Bearing customizable model*, printed with a slicing trick. The print settings used are the same as in Table 1, except the infill percentage was set to zero. The main motivator behind the Mark 3 drivetrain was to generate our own geometry in a CAD program in order to give us more design control, while still employing slicing tricks to create the final elastic properties of the part. The Mark 3 gear belts come from a ring gear CAD model that we created, but only the inside surface of the ring gear was modeled – the outside surface is a result of the slicing trick (Figure 25 and 26).

More traditional belt-drive components may produce a resilient enough drive system (Figure 29), while putting less of a demand on the borehole wall by eliminating the "clicking" motion caused by
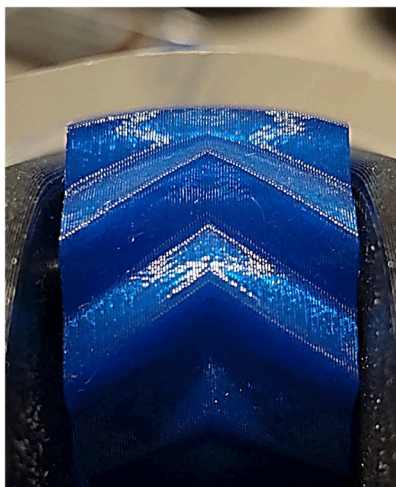

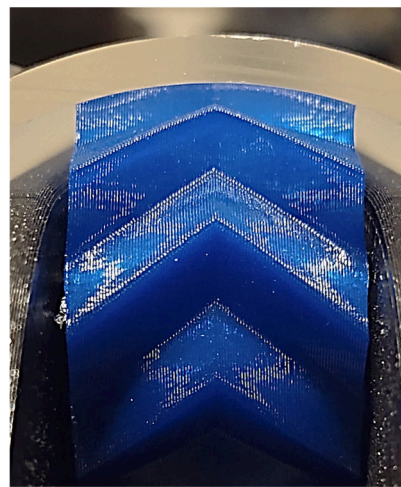*Figure 23 (left): Gear deforming to match the contour of the bore.*
Figure 24 (right): Gear with belt installed, conforming to the bore contour.

some of the more aggressive gear teeth. In both the gear-drive and belt-drive varieties, directional drilling may be achieved by deflecting one end of one track(s) out to provide an axial deflection in the borehole. Currently, we are moving the architecture forward using both gear and belt drive.

The largest challenge faced by the borebots architecture is power consumption. Therefore, the system must be designed to balance mechanical, thermal, electronic, and power storage considerations in order to guarantee the level of performance required to reach the target depth. Testing will be required to determine which drive system methodology is preferable. Energy efficiency is the primary motivator in this selection, but system robustness should be weighed in the decision as well.
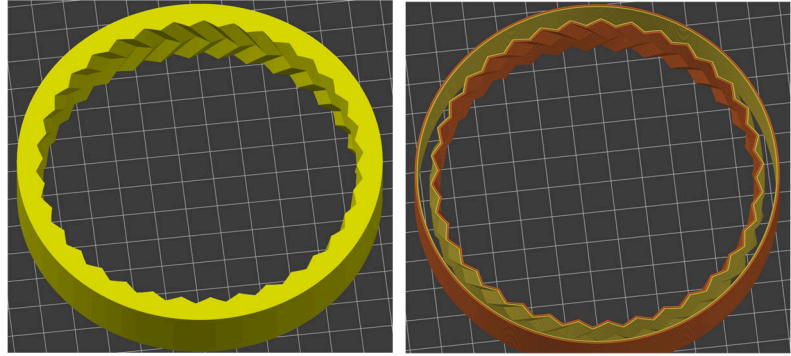

Figure 25 (left): Mark 3 ring gear model loaded into PrusaSlicer.
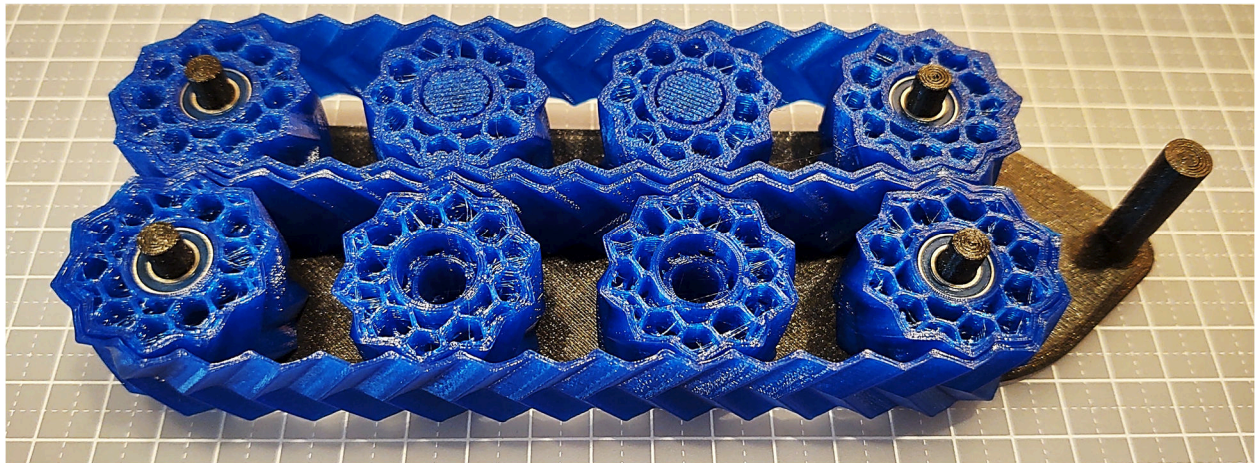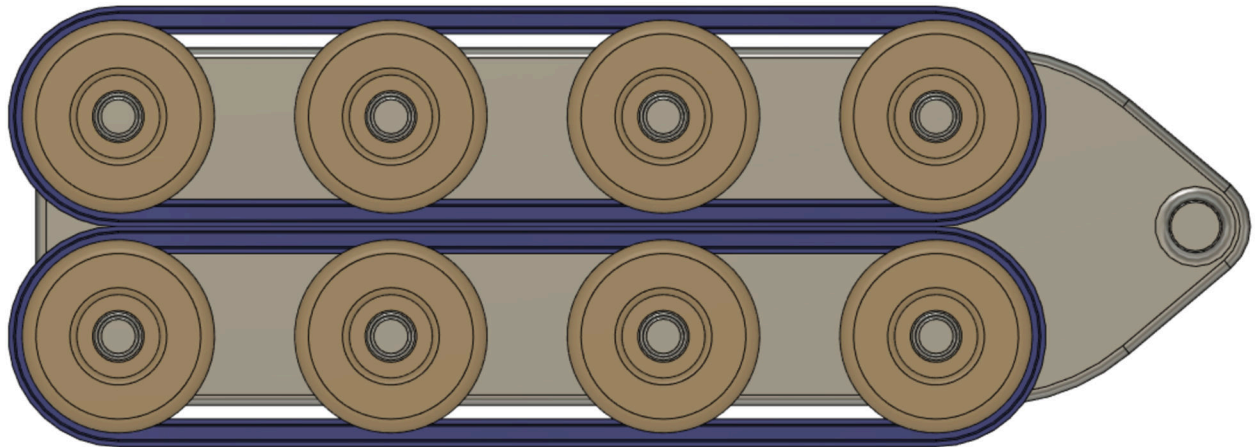*Figure 26 (right): Sliced ring gear, showing exterior belt surface.*

Figure 27 (top) & 28 (bottom): Mk 3 gear-belt drivetrain prototype module, and a flat-belt/flanged-pulley mockup.

For the flat belt drivetrain (Figure 28 & 29), there are three options worth considering, which are shown side-by-side in Figures 30, 31, & 32. The first two types both rely on crowned pulleys, and the third uses flat pulleys with a flange. Crowned pulleys are commonly seen on belt sanders today, and used to be common in lineshaft machine shops (Matthews, 2005). Flanged pulleys are frequently used in robotics; however, the flange would normally interfere with the bore in this case. The
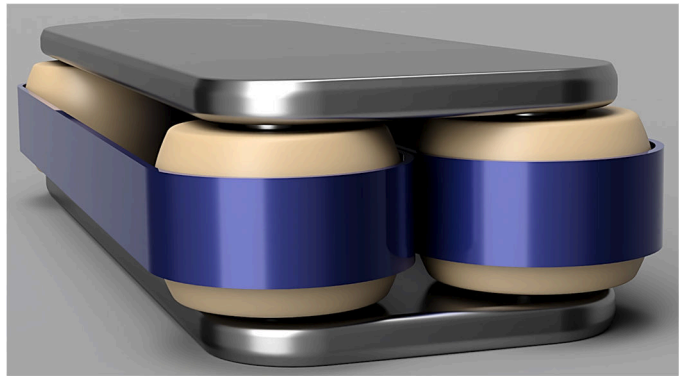

Figure 29: Mockup prototype module of a flat-belt drivetrain. The crowned shape of the pulleys provides a centering force when the belt is deflected off the centerline of the pulley.
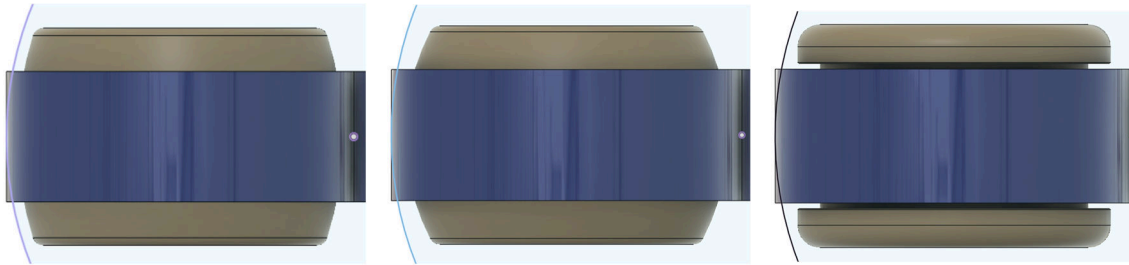
parameter space for this type of flat belt drivetrain is actually complex, with the rolling resistance, centering force, size requirements and power transmission all playing a role. A standard flanged pulley would come in last place on nearly all marks if off-the-shelf components were used: the risk of high friction when the belt goes off-center and crowds the flange, no centering force beyond the constraint of having a flange, the larger diameter required for the flange causing interference with

Figure 30, 31, & 32: Mark 3 flat-belt drivetrain mockups: crowned pulleys left and center; flanged pulley at right.

the borehole, and the impracticality of having the belt transfer the drive power from one track to the other via the center belt-to-belt contact region as with the other options (and with the gear belt options). However, if the belt is made extremely thick it can overcome these challenges using a conventional (but uncommon) type of flanged pulley. The crowned pulleys don't really need much more of an explanation: either they will prove themselves useful during testing, or they won't. The flanged pulley, however, has a much more uphill battle, and the new type of thick belt still needs to be fully described, prototyped, and tested. See Matthews (2005) for more on flanged pulleys.

Figure 33 (left): Cross-section of the crowned pulley and thick belt, designed to minimize crowding of the flange.
Figure 34 (right): Mockup flat-belt drivetrain prototype module using flanged pulleys and a thick belt.
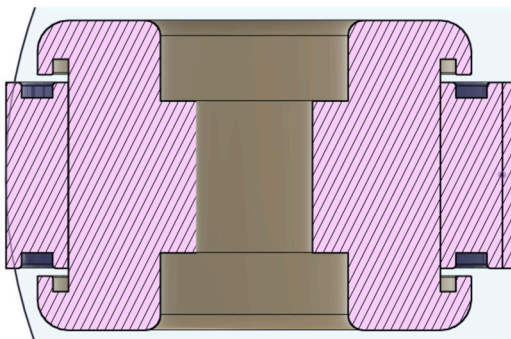
There are several options for powering the borebots drivetrain. However, we will be focusing on a simplified chain-drive version for the next (first truly self-propelled) borebot prototype. The original Mark 1 prototype used a rubber belt and an integral pulley, added to one of the gears with a Boolean operation (Figure 35). This can also be seen in the video linked to earlier (https://git.io/JBbJ1) and in Figure 13 (the black gear). This configuration proved cumbersome and unreliable for testing. Although

Figure 35: Mk 1 components in their approximate locations. The blue gear and pulley are a single piece, and are powered by the red pulley. The belt connecting them is omitted for clarity. See also: Fig. 13.

a rubber belt may be the ultimate solution, using #25 chain can allow for a lower-profile component stackup and more reliable interface for prototyping work (Figure 37). Other notable drive options include a "direct" gear-drive that acts on the outer surface of the gear-belt, and a
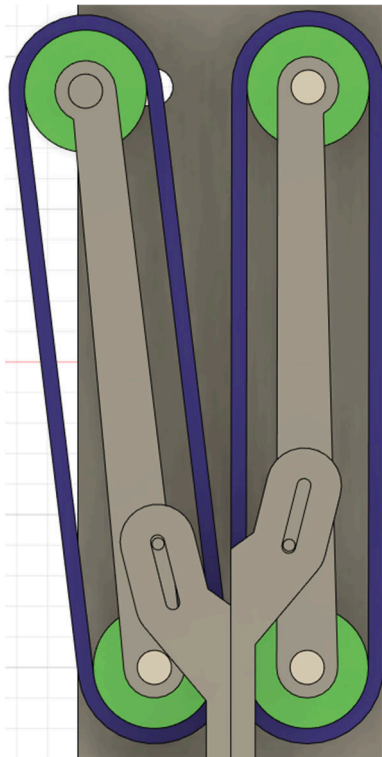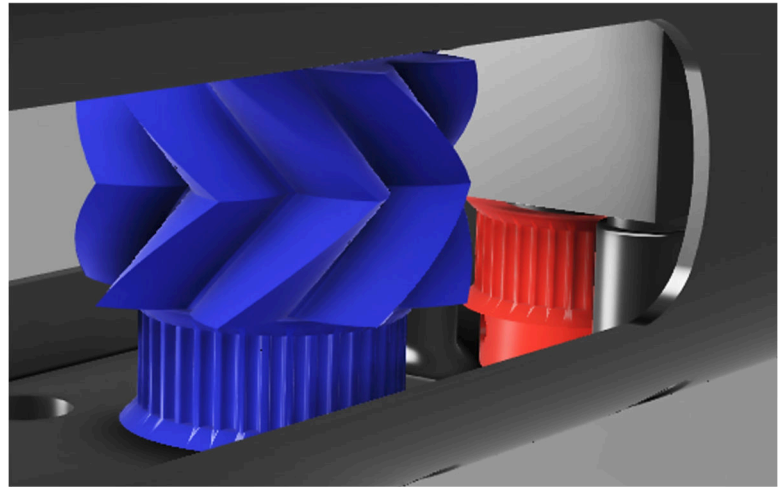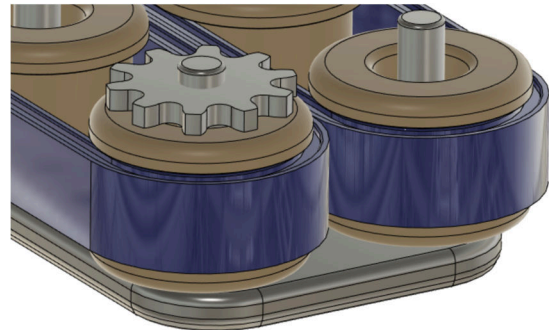

Figure 37: Sketch of a sprocket for chain drive

worm drive configuration in which the worm gear would be placed between the two gear-belts. The power modeling that is currently in work – and the lessons learned from the chain-drive prototypes – will help to focus our efforts, and define a range of motor power requirements.

Figure 36: An early sketch of a variable pressure drive, with enough deflection to "steer."

The borebot will be responsible for providing the Weight on Bit (WOB) needed by the drill, the effective pressure against the borehole wall (either by design or by active control, see Figure 36), and will also need to provide attitude corrections to maintain the straightness of the borehole. While WOB and pressure have been touched on previously, the concept of "steering" adjustments makes the situation more complicated, and further makes the case for mechanical control of track pressures. It does appear that having a variable-pressure drive can increase drivetrain efficiencies overall (and still provide good traction for WOB demands during drilling), so this consideration alone may make it the more desirable choice.

Drilling

Generally speaking, any drilling head can be used with the borebots system if the drill head in question can be made to match the diameter of the borebot (which itself can be modified). The size of the borebot could be increased to match a drill head if it had advantages over other options. The size of the borebot was chosen to represent a practical lower diameter limit and to align with existing drill heads in the NASA technology pipeline (like the Planetary Deep Drill mentioned previously; see Zacny et al., 2016). That said, there are unique limitations to the borebot system that merit the design of a unique family of drill heads specifically tailored for integration into the borebots architecture. The two main limitations are the Weight on Bit (WOB) available to the drill head (as the drivetrain must supply nearly all of the WOB experienced by the drill), and drilling efficiency. If drilling efficiency suffers, the drilling process will have to be cut short in order to leave enough power available for the return trip.

The design of drill heads for the borebots architecture is a secondary consideration for this project, and is mainly undertaken to provide a jumping-off point for mission planners. The modification of existing drill heads can be undertaken to reduce WOB requirements while keeping drilling efficiency reasonable. The authors do not claim to be drilling experts; however, we note that conventional drilling wisdom (Talalay, 2014) does not fully align with the most optimal cutting geometries as described in Ueda & Kalafut (1989). This misalignment may be due to the "luxury" of high WOB, combined with the power availability inherent with heavy tethered (read: surface powered) systems. This is the logical basis for the development of an annular drill head with a 30-degree cutting angle for use with the borebots system. We then bifurcate this drill head into two versions, one with a thicker annulus and one with a thinner annulus. The thicker annulus allows room for a unique core breaking and retention mechanism, while the version with the thinner annulus uses a more traditional "core dog" retention device.

The drill head with simple core dogs is shown in Figure 38. The core dog retention devices were based on Figure 40 (Talalay, 2014, fig. 25). The location of the core dogs is shown in detail in Figure 39. It should be noted that this is just one option for core retention; this configuration is simple and robust, but difficult to manufacture. With a diameter of 64 mm and a core diameter of 45 mm, breaking the core usually isn't the hard part – holding on to it is. To mitigate the challenges of retaining the core (especially when the composition is uncertain), a spherical iris cutting and
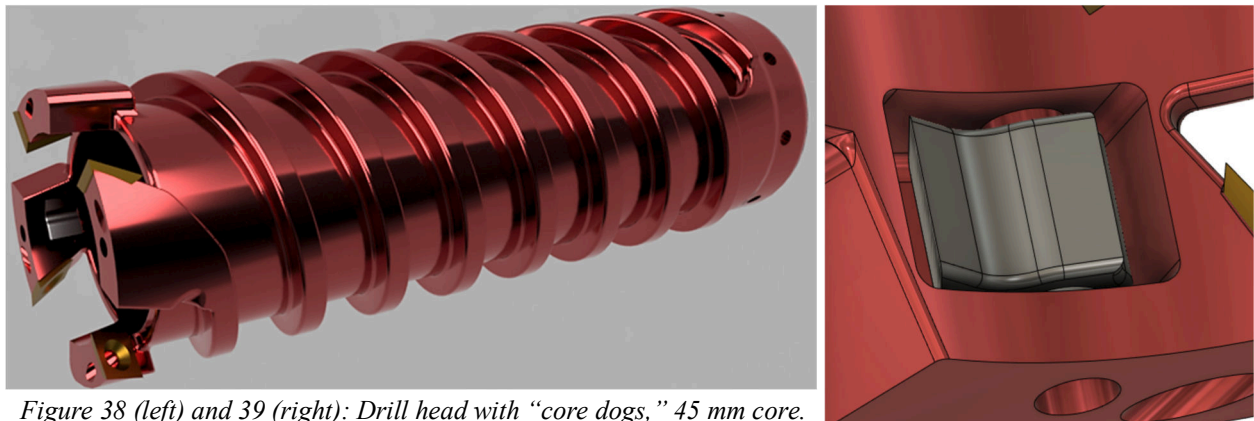

Figure 38 (left) and 39 (right): Drill head with "core dogs," 45 mm core.
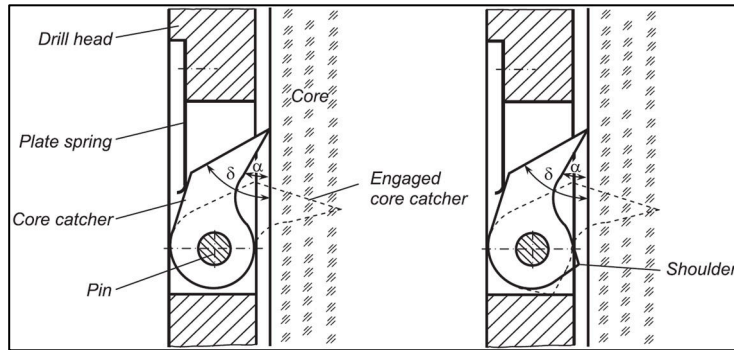
Figure 41 (bottom left): iris core retention mechanism in the closed position. Titanium-Nitride-coated (gold colored) Carbide tips can be seen on the iris blades at the center.

Figure 42 (bottom right): iris core retention mechanism in open position. The mechanism reduces the core diameter to 40 mm.
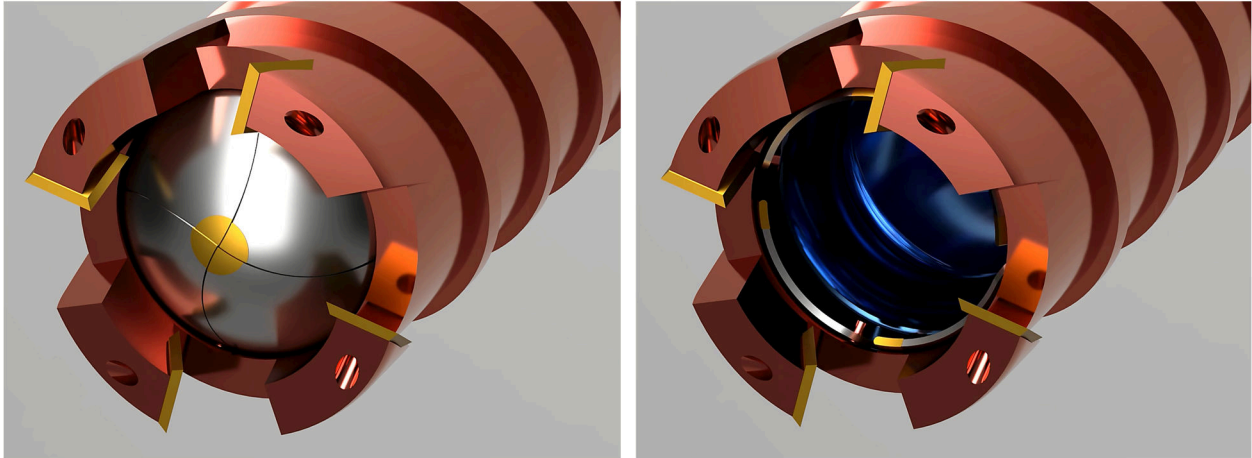
retention mechanism was investigated (Figure 41, closed position; Figure 42, open position). The device can be seen with the outer (red) part of the drill hidden in Figure 43 and 44. Two animations of the iris closing action can be downloaded from https://git.io/JsKah and https://git.io/JsPov.

To accommodate the iris mechanism, the effective core diameter drops to 40 mm. Actuation of the iris is provided by the inner barrel (shown in blue), which can be locked to the borebot body via deployable pins in the front of the borebot. This can allow the drill motor to rotate the outer barrel (red) while the blue barrel remains fixed, providing the motion necessary to close the iris. The iris mechanism is based on a preassembled iris box (Lalish, 2016; Kerr, 2016), and was published on Thingiverse.com to respect the open-source license (Morley, 2021).

Figure 43 (left) and 44 (right): iris mechanism with red part of drill hidden. Blades pivot around hole at fwd. end.

There are several advantages to this kind of a core breaker and retainer. For one, it can retain unconsolidated material or severely broken cores, while only reducing the overall core diamet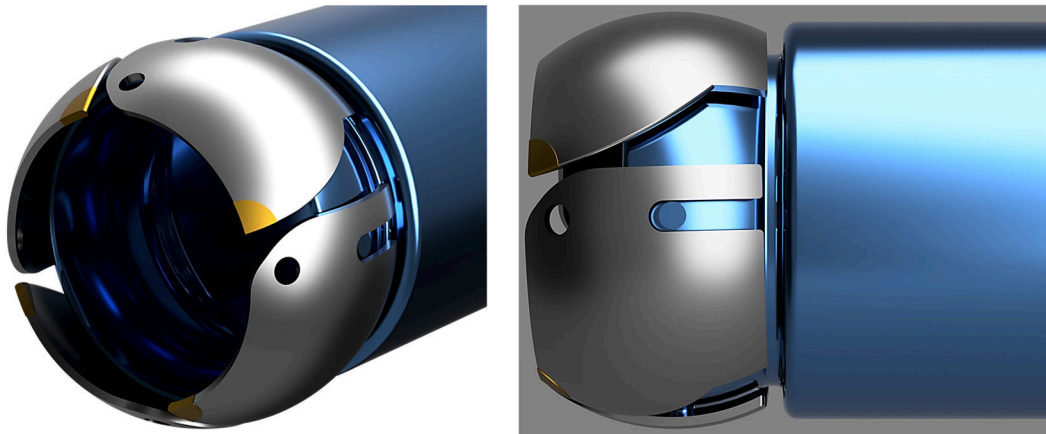er by 5 millimeters. It is also possible to use the iris to incrementally cut solid cores, turning the core-breaking step into a machining procedure instead of a fracture procedure. This can reduce the required torque to initiate a break, which helps make a borebot with only a single pair of tracks more feasible. The incremental core-breaking process would require the installation of the ratchet in the aft end of the drill head, and there is adequate room for such a device. It is possible to reset the ratchet (after the iris is closed) using a few methodologies, the simplest being the operation of an electric solenoid via the electrical connection integrated into the borebot main coupler. Another method may be to only deploy a single pin puller (instead of the pair of pin pullers at once), thereby offering an analog mechanical input that can reset the ratchet. Another method could allow for the ratchet to lock with slight counter-rotation, but to disengage with half-turn counter-rotation. Other methods are possible, these are offered as robust examples that fit the available space. Future prototypes are likely to feature ratchets that require a manual reset, to facilitate testing.

The presence of the inner barrel (and control over it) can help prevent chips and fines from packing in both the throat of the drill head and the hole at the top of the flutes (all cuttings are to be routed to the central chamber of the drill head, where room is available aft of the core for cuttings storage). This may potentially have a benefit even without the iris core retention, as smaller and more frequently-spaced holes can be added along the flutes to route material into the center chamber of the drill head, and these holes would match up with corresponding holes in the blue inner barrel. When the inner barrel is rotated, it could operate like a cheese-grader, bringing the cuttings into the central chamber (it may be desirable to add punched "scoops" to the inner barrel to accentuate this effect). This "cheese-grader" functionality has nothing specifically to do with borebots, it is simply a benefit to having an actuatable inner barrel. It will not be explored further, although the iris drill head will benefit by having the inner barrel available to keep the cuttings hole clear (video animation at https://git.io/JXkI8).

The WOB available to / required by the drill is still unconstrained (although Ueda & Kalafut (1989) is encouraging). Due to lower gravity on Mars, it is wise to design the system such that 100% of the required WOB comes from the drivetrain. The borebot mass (on the order of 10 kg) may not be sufficient. WOB is a parameter for optimization, as the requirement at the drill head drives the normal force required of the drivetrain against the borehole wall. If, for example, 1000 N of WOB is required, and a 0.25 coefficient of friction is used, the following normal force would be required from each track pair:

$$f_{friction} = \mu F_{normal} \quad \rightarrow \quad f_{friction}/\mu = F_{normal} \quad \rightarrow \quad F_{normal} = 1000 \, N/0.25 = \mathbf{250 \, N}$$

Practically, this would equate to a preload (when the tracks are squeezed to conform to the borehole diameter) such that the resulting normal force (from the Hooke's law behavior of the track/gear material) is 250 N total, or 125 N per individual track. This may be a good reason to use a variable-pressure track system, as such a normal force would not be required during driving, and would increase the friction in the drive system. This would then become an optimization parameter and could be leveraged with the approach discussed in Joshi (2021).

Power and Components

The Mars helicopter technology demonstrator Ingenuity has shown that relatively low-cost Commercial Off-The-Shelf (COTS) hardware can survive (and thrive) in Martian conditions. The thermal management used on Ingenuity is the best example we have for polar operations during the summer (Cappucci & Moulton, 2018). The borebots architecture potentially has a few advantages over Ingenuity, but some of them may come at a cost. For one, we have the opportunity to store borebots back in their flight-stowage location where they can enjoy an amenable thermal environment and a power link to the rover. This complicates the storage functionality, so it should be considered a last resort. It is true that the harshest conditions a borebot is likely to face are at the surface, so it is an option that should be kept in mind. Battery charging is possible when loaded in either the assembly station or the cleaning station, but there is no protection from the temperature at either location. Heaters inside the borebot can likely compensate for this. Another advantage is the time spent inside the ice (believe it or not). The ice can protect the electronics from solar and cosmic radiation, and provide a much more predictable thermal environment. It is estimated that the base of the ice sheet has a temperature between 180-200 K (Buhler, 2021; Sori & Bramson, 2019), which is approximately equal to the design criteria used for Ingenuity (Balaram, 2021; 2018).

The body of a borebot has an inside diameter of between 55 mm and 60 mm, which (generally speaking) can fit batteries in groups of five in that space. The battery that we are looking at in-depth is the tried-and-true 18650 lithium-ion cell (Darcy & Scharf, 2015; Walker, 2017). Two groups of five batteries appears to be the minimum logical energy storage option for a borebot. However, we have the option to add up to five groups of five batteries before storage of borebots on a rover becomes impractical. The fewer batteries contained in each borebot, the more borebots total can be brought in a given spacecraft. Preliminary power modeling shows that there does not appear to be a penalty for increasing the energy storage capability in borebots. The available spacecraft storage, manipulation capability, and recharging ability are the primary reasons to limit the number of cells to between 10 and 30 per borebot. The amount of heat needed to keep the batteries above zero Celsius (the lower practical limit for most chemistries) is watt-order, and is still poorly constrained. A sketch can be seen in Figure 45 which shows two groups of five cells, separated by a 1-watt radioisotope thermal generator (RTG) to help keep the batteries warm.
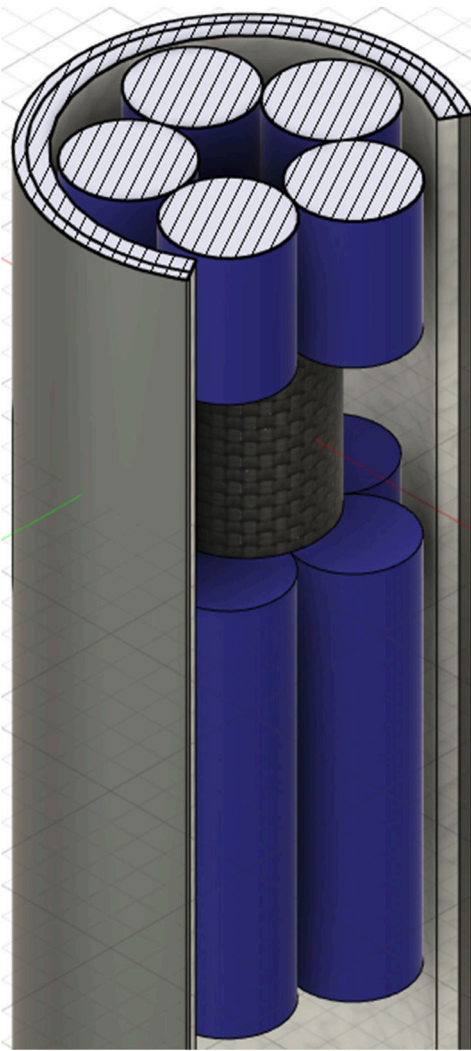

Figure 45: Ten 18650 Li-Ion cells and a 1-watt RTG to keep them warm.

Depth (m)	Number of Trips	Drive Time per Trip (min)	Cumulative Distance (m)	Trips per Bot
1	7	1	8.40	1
10	67	2	683.4	6
50	333	4	16,683	28
100	667	8	66,833	56
200	1,333	14	266,733	112
500	3,333	34	1,667,000	278
1,000	6,667	68	6,668,000	556
1,500	10,000	101	15,000,000	834

Table 2: Logistics of drilling a 1500 m borehole with 12 borebots. 150 mm core length, drilling time neglected.

The logistics of deep drilling with multiple borebots can boggle the mind when considered at scale. However, the concept does appear to stand up to rigorous analysis. During the final months of the NIAC study we hope to dial-in some of our unknowns and better constrain the parameter space. Optimization of the borebots system will be complicated but rewarding, as the plot below shows (Figure 46). The system is sensitive to very small changes, notably: friction in the drivetrain, hotel loads from onboard electronics during the drive, drive speed (which makes hotel loads higher-impact on longer drives), and available onboard power.

Figure 46 (below): Early power modeling with two-to-seven packs of five 18650 cells each. Assumptions: driving and drilling consume 30 watts each, with a 15 watt electronics hotel load, core length of 150 mm, 37.5 min. drilling time.
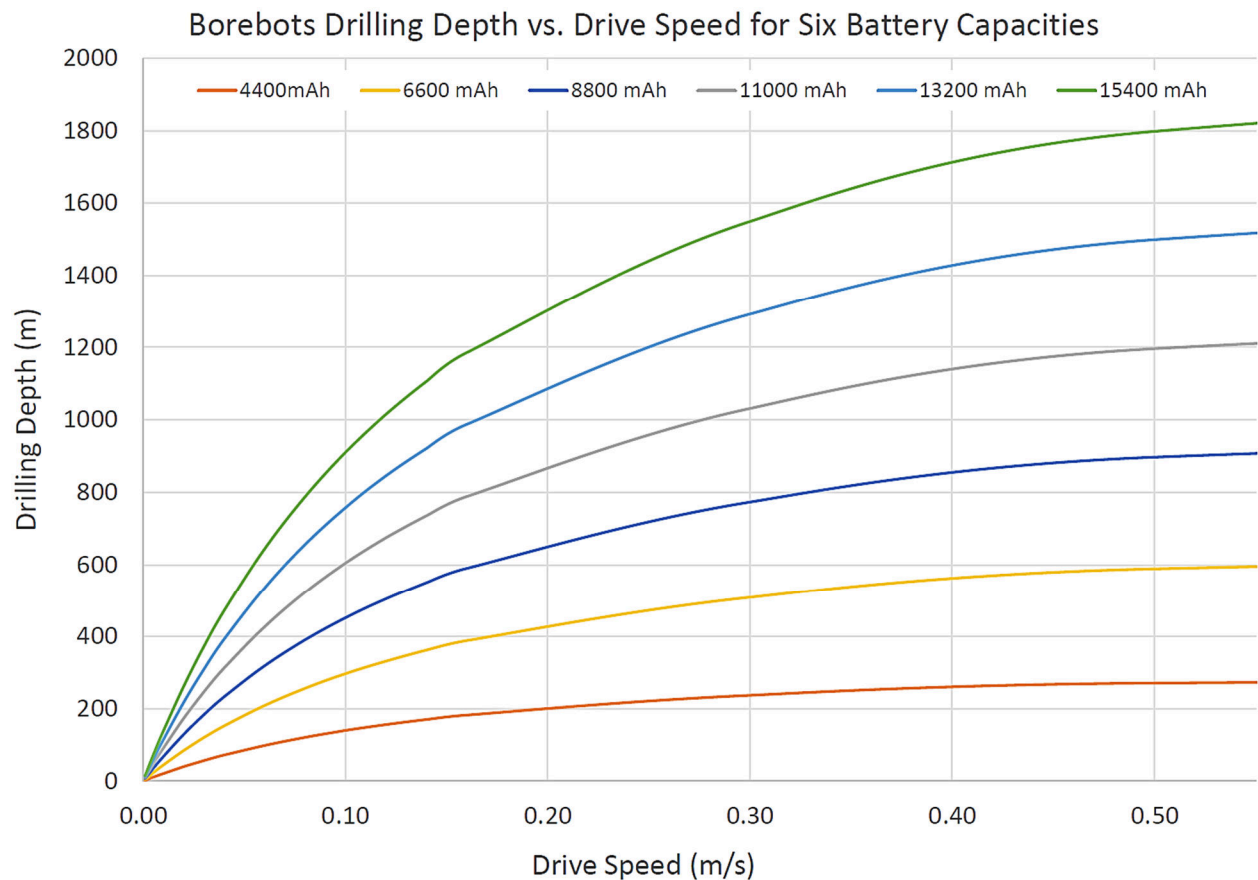
Alternate Borebot Architectures

A 2003 report by The Committee on Planetary and Lunar Exploration discusses the challenge of learning about the past climate of Mars, emphasizing the importance of returning samples to Earth:

> "Learning about the past climate of Mars is another important objective of Mars science, and returned samples offer the best way to understand an important product of past climates. Ultimately it may be possible to return ice cores from the martian poles that directly address the planet's climate history…" (National Academies, 2003, p. 84).

Just pages later they recommended "on the order of 10" sample return missions during the Mars Sample Return (MSR) campaign (pp. 101-102), hopefully featuring deep drilling to reach below the radiation-afflicted surface to search for clues about past life and climate. This is clearly reminiscent of the "cheaper, faster, better" days of JPL, but was unlikely to be plausible in the post-reassessment era, following the tragic loss of the Mars Climate Orbiter (MCO) and Mars Polar Lander (MPL). Little did they know that the "2011 sample return mission" they spoke of would in fact land during 2021 at a cost of $2.5 billion (The Planetary Society, n.d.).

The thought of ten Perseverance rovers being deployed to the most science-rich parts of Mars is tantalizing, and in 2021 we must try not to laugh at the political and financial impossibility of such an undertaking. On the other hand, we must not stop pressing forward with deep drilling technology development when told that Flagship missions are too expensive to pursue. In the span of twenty years, ten missions may have become impossible, but we refuse to believe the number has dropped to "one-and-done." Even if human colonization of Mars is successful as the century presses on, robotic exploration and MSR have their place. In that context, it could be argued that polar science is one of the most logical places for robotic science missions to target.

Although this investigative team doesn't believe in the practicality of ten missions nor the impossibility of "one more Mars flagship," we see many other possible versions of the borebots architecture, and all of them are cheaper. Our work so far has really shown us the advantages of using a Perseverance-twin; it appears to be the lowest-risk option with the longest potential mission life. However, the alternate architectures outlined in this chapter all feature ways to mitigate the risks inherent to smaller, low-cost missions. Redundancy and flexibility are something all borebot architectures have in common, and these alternate architectures are thusly robust and capable.

Small Static Lander

The success of the Phoenix and InSight landers have shown that static lander missions can have a significant science return at low to medium cost (Lockheed Martin, n.d.). Using a build-to-print lander could allow this class of deep drilling mission to compete in the NASA Discovery Program. This makes a mission more likely to get selected; however, it does trade financial risk for higher mission risk. The Heat Flow and Physical Properties Package (HP^3) on InSight shows us that drilling on-the-cheap is not easy, and that the risk intrinsic to these low-cost missions is very real. The mole probe, which is the centerpiece of the HP^3 instrument, failed to penetrate into

the martian regolith properly, and is stuck just centimeters below the surface (Jet Propulsion Laboratory, 2021). We believe the borebots architecture can provide a more resilient capability, and that a static lander could make significant progress drilling into the Polar Layered Deposits (PLD). This could allow both PLDs to be explored at less than half the cost of a single, large-rover deep drilling mission.
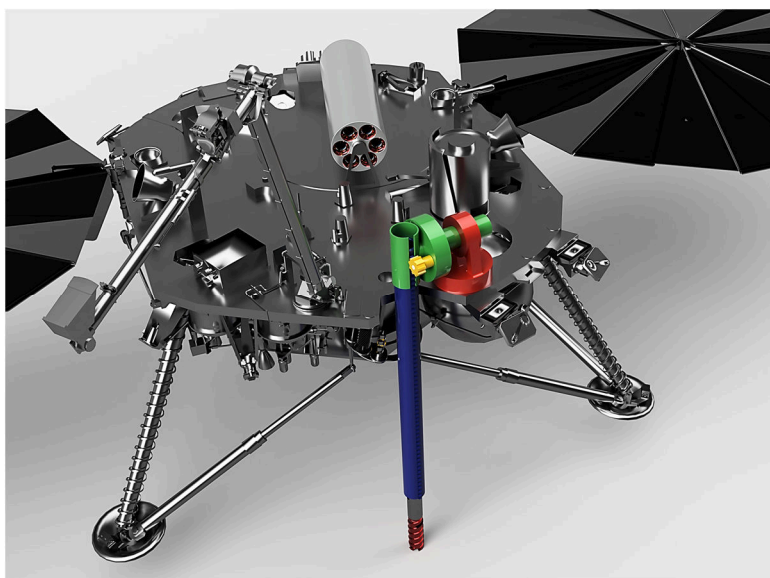

Figure 47: sketch of a static lander with a 3-DoF deployment tube.

The downside of this architecture is that drilling all the way to the basal unit is highly unlikely, due to the reduced capabilities of a static lander, combined with the shorter lifetime when using solar power (although, the MPL may have been capable of surviving winter; see Clifford et al., 2000, section 3.3). Relocating for an auxiliary extended mission is also impossible, however, a second borehole may be possible (at an angle).

In this lower-cost context, a specific ice core analysis suite does not seem cost effective, and instead very small samples from ice cores (like the dust from the cleaning process) could be routed to instruments like TEGA and MECA from the Phoenix Lander (Smith, 2005). With this type of mission, the motivation for core retrieval is lower energy consumption during drilling and the easier removal of material from the hole (and the drill head). It can be difficult to remove chips and dust from full-faced drills, so the coring strategy developed for the large rover architecture still has advantages here. It is worth noting, however, that a full-faced drill head could be attached to a borebot (the drill head used in this chapter is a strawman; any small/light drill head could be used). The example static lander in this section is based on the MPL / Phoenix / InSight platform, since the Phoenix science payload is very capable and could be re-flown in its entirety, saving additional money by using build-to-print instruments. Few modifications to the lander will be required. Efforts should focus on modernization and miniaturization of support systems to increase usable payload volume and overall power capacity.

To integrate the borebots capability into the lander, a three-degree-of-freedom deployment tube is added adjacent to the robot arm as shown in Figure 47. The tube is pre-loaded with a fully assembled borebot, and provisions to recharge the borebot in the deployment tube itself should be provided (i.e., side-mounted contacts). A cleaning station can be added under the deck of the lander (Figure 50), and plumbed into the pneumatic sample handling system as discussed previously (Zacny et al., 2019). This first borebot will operate by itself for as long as possible, taking many cores and dumping the excavated material out under the lander (directly under the cleaning station). The entire volume of material removed from the hole will be about a quarter of a cubic
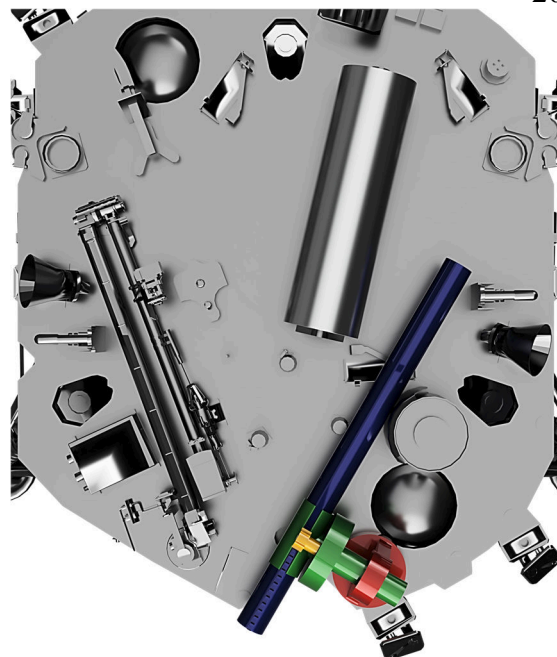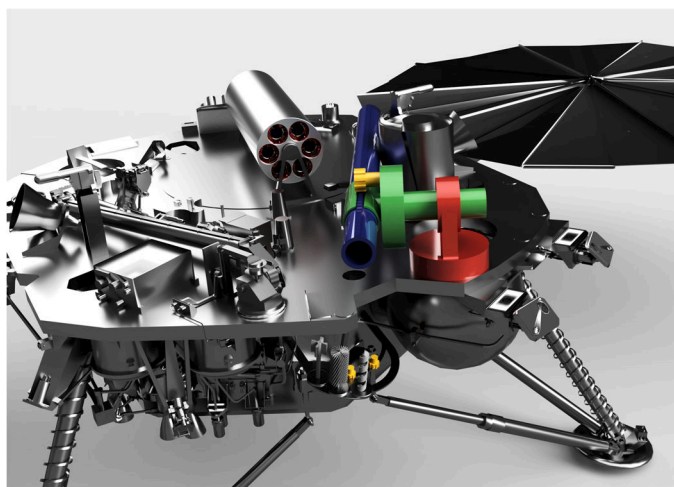
Figure 48 & 49: stowed configuration of deployment tube. Carousel containing six spare borebots is shown. Deck space is available for downhole / deck-mounted science instruments.

meter at the completion of the primary mission. Considering this, the robot arm may be best used as a "cleaning assistant" to move material away from the borehole, and can also occasionally position itself under the cleaning station to capture a specific portion of a sample. The arm could also be fitted with a special scoop to take a piece of an ice core out of the drill head part-way through the cleaning process.

Spare borebots (up to six spares, in addition to the one pre-loaded in the deployment tube) can be included, and could be stored next to the deployment tube on the rover deck. One option for this is a revolver-style borebot container is shown in (Figure 48, 49 & 50). A second container (not pictured) could house downhole science instruments, or the space on the deck could be used for other science instruments. The pre-loaded borebot would be either be placed on the deck or discarded on the surface when it has exceeded its useful life (using the robot arm to push it out of the way). If the borebot being replaced is completely dead, the spare borebot being loaded could be used to push its deceased companion out of the tube. It may be wise to provide an electrical path between the tube and borebot for the purposes of firing pyros within a dead borebot, in order to sever the mechanical links in the drivetrain (this may be necessary for the spare borebot to push a dead borebot out of the tube). The same connections as the charging circuit could be used, but the pyro circuit could be sensitive to a sustained voltage spike.
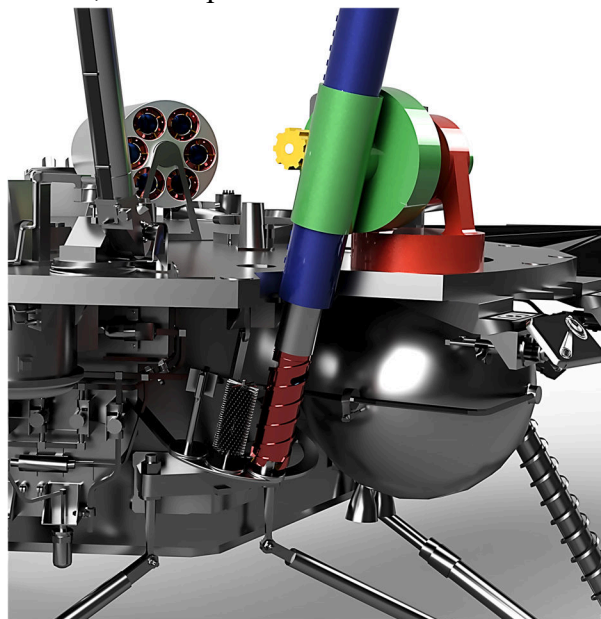

Figure 50: cleaning station under the lander deck.

Small Rover

A Mars Exploration Rover (MER)-class mission could provide a low-cost mission profile that could mitigate some of the risks of the static lander mission by being mobile. Using build-to-print components, it may be possible to fit a mission of this class into a Discovery Program budget. To integrate the borebots system into an MER-class rover, it may be best to forego the mast entirely and install a 2-DoF deployment tube in its place. If the MER science strategy is followed, the robot arm will be responsible for the majority of the science duties (NASA Mars, n.d.). Lessons learned from Perseverance's turret instruments could be applied here, in miniature form. The arm could examine chips and fines from the cleaning process before scooping them out of the way. A cleaning system similar to the previous section is envisioned, which makes fitting a robot arm a challenge due to the limited room for stowage (Figure 51 & 52; robot arm not shown). In order to offer drilling redundancy, the deployment tube could be a "double-barrel" design. This mission class shares the short life and lower power availability with the static lander concept.

Figure 51 (above): MER-class small rover with a 2-DoF double-barrel deployment tube, shown during a drilling operation.

Figure 52 (below): Stowed configuration of double-barrel deployment tube. Stowed cleaning station can also be seen.

To make up for the decreased science payload intrinsic to small rover missions, a downhole instrument suite may be the best way to increase science return. Perhaps the second deployment tube could be used to deploy a borebot fitted with downhole science instruments. The rover could maneuver the main deployment tube over the hole for drilling operations, and maneuver the second deployment tube over the hole to deploy the science borebot. This complex mode of operation would increase up-front costs, but offer an increased science return without substantial changes to existing rover designs. Another option may be a simplified microscopic imaging
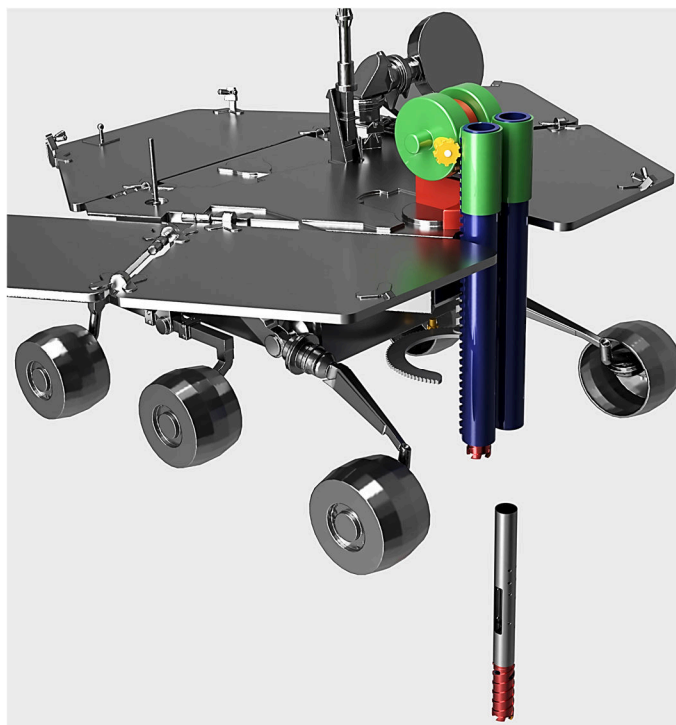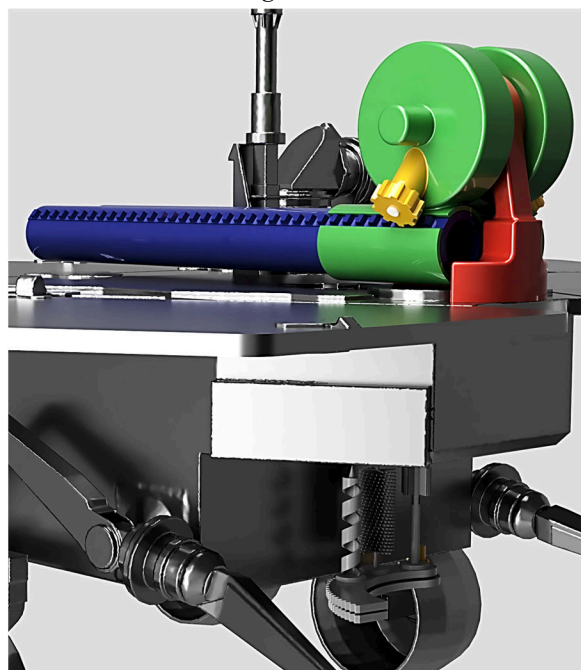
module (UV/optical; Zacny, 2016), that can be built into the borebots themselves. Future work on integration could choose to retain or omit the robot arm for this mission class. Stowing the front wheels, cleaning station, and robot arm in the available space will be a challenge.

To mitigate the risk from the external science payload options, a SuperCam-esque instrument (Maurice et al., 2021) could be permanently affixed adjacent to the cleaning station (under the rover deck). This may not be compatible with the presence of the robot arm, but may be more useful in practice. It could feature a very limited 2-DoF range of motion, in order to analyze dust and chunks of ice core from a distance. The main challenge of an MER-class mission

Figure 53: MER-class rover using a strawman cleaning station. Note that the front wheels, cleaning station, robot arm, and a camera module all would need to occupy this space during flight.

then becomes a game of miniaturization and integration. Can we fit two deployment tubes in the mast volume? Can we add enough science to the small and weak robot arm? Can we add a significant remote science payload (SuperCam) to mitigate risk if the external science payloads fail or have a low return? Do we have to remove the robot arm to make room for the cleaning station and SuperCam? These challenges are substantial. The advantage of mobility will need to be weighed against these risks during future work. Having the ability to abandon a drilling site (and even a borebot), and begin operations at a new location makes this system much more flexible. The limiting factors here would be the available rover power and borebot longevity (including the drilling head). Because of these limits, extended missions in this mission class should focus on additional boreholes, not greater depth, in order to maximize science return within the limited power and component lifespans.

One interesting note on an auxiliary extended mission profile: it was recommended by a previous decadal mission concept study to use small rovers to perform spectrometry work on excavated material in polar regions (Calvin, 2010, p. 21 para. 5). There may also be a benefit to drilling several shallow holes while traversing down a slope (Clifford et al., 2013, section 3.1). If the external science payloads fail, the rover could focus on mobility and near-surface sampling. It is likely that the deployment tubes could be used to dig trenches during this kind of a mission, even if (or after) all of the borebots have died. The MER rovers also used their wheels to dig trenches at times (NASA, 2008). If a suitable SuperCam-esque instrument can be integrated into the front of the rover (or mounted to the outside of the deployment tubes), this would be a very substantial auxiliary extended mission goal, and one that isn't available to a static lander. This mission phase could continue until polar winter seals the rover's fate.
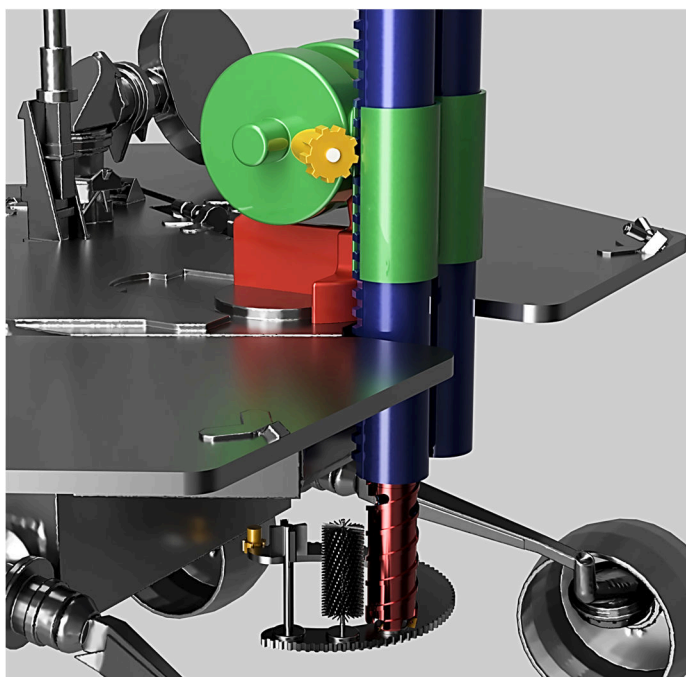
Small Rover + Static Lander Combo

This concept combines the first two alternate architectures into a packaged New Frontiers mission, on a single launch vehicle. A defining feature of the static lander in this case is the inclusion of a multi-mission Radioisotope Thermoelectric Generator (mmRTG), which can enable over-wintering. The static lander would be well-equipped with scientific instruments, de-scoping only what is required to physically fit the mmRTG. Sample handling can be primarily pneumatic (from the cleaning station), with the option to have the rover use the cleaning station on the lander in order to offer samples to the pneumatic system. A strategy could be developed that would enable the small rover to "dock" next to the static lander, and connect a power umbilical to keep the small rover alive through winter. This concept may be able to achieve basal unit access if enough borebots can be brought along, and is presented as a second potential way to achieve that goal during extended operations.

It may also be possible to use this configuration for a more expensive mission and integrate the Perseverance ACA into the static lander. JPL designed the ACA to be modular, so the mission would lose most of the build-to-print heritage of the lander platform but gain the valuable ACA heritage (Schaler, 2021). This may result in a lander that is still half the cost of a Perseverance twin, and perhaps the cost savings could be allocated towards expanding the Mars Sample Return program, possibly even upgrading the rover assistant to a sample return rover (with launcher).
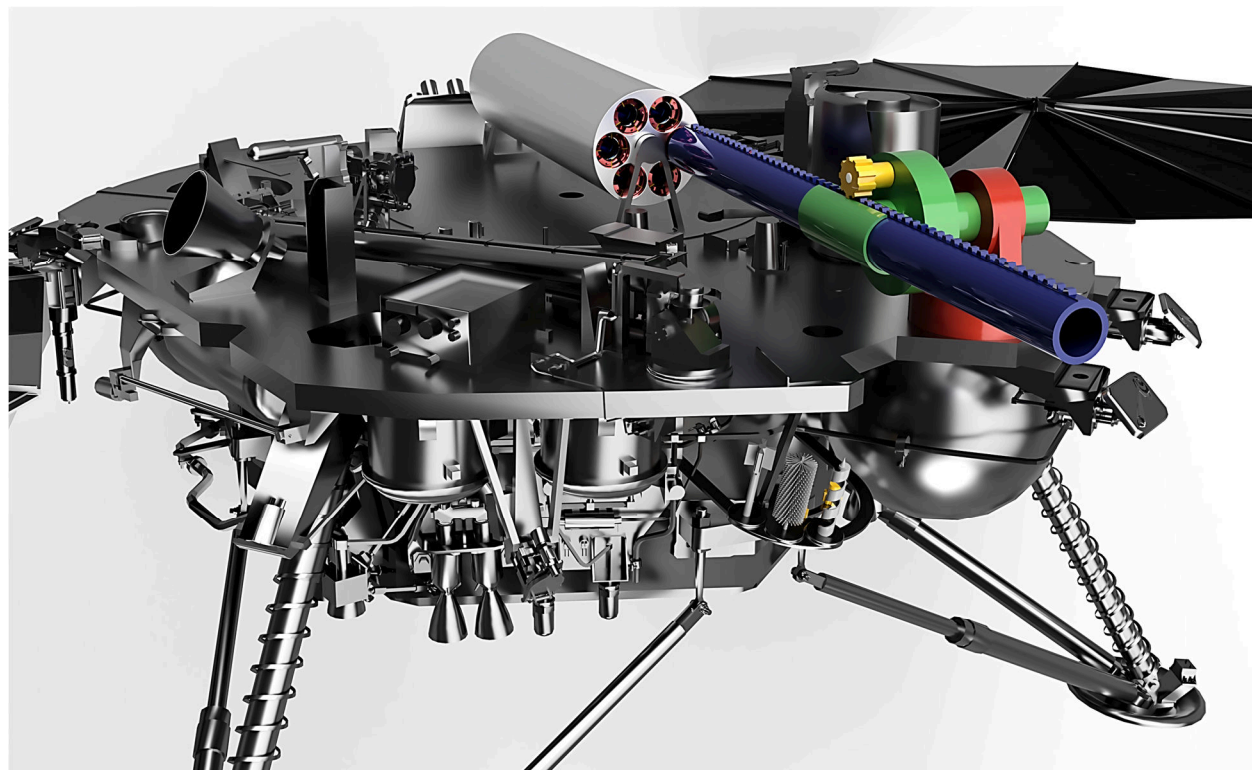

Figure 54: The deployment tube of a static lander in position to receive a borebot from storage. Note that a similar dispenser could be stored directly to the left of the one shown, which could hold downhole science instruments pre-installed on borebots. A weather station or other instrumentation could be added elsewhere on the deck.

Commercial-off-the-Shelf Robots

NASA has been looking at ways to explore caves with COTS robots, as exemplified by the NASA Biologic and Resource Analog Investigations in Low Light Environments (BRAILLE) project, shown in Figure 55 (Sleater, n.d.). The end goal here is to enable the exploration of lava tubes on our Moon and Mars using these systems. This work could be leveraged and applied to a Borebots context. The existing team-based approach to cave exploration could be augmented for use in polar science,

Figure 55: Boston Dynamics Spot robots exploring a cave. Photo Credit: Nasa/BRAILLE Team, (Sleater, n.d.).

limited to a single summer season. By adding additional robotic team members designed to perform drilling activities, an extremely low-budget deep drilling architecture emerges.

Figure 56 shows a sketch with three possible Boston Dynamics Spot robot configurations that could be added to the existing team dynamic in order to perform deep drilling work (Spot 3D model credit to Great, n.d.). A roll-out solar array could be fitted with charging docks for the Spot robots, perhaps with drill cleaning stations between the charging docks. With a $75,000 list price, Spot robots offer the lowest-cost way to explore the polar regions for a single season. It may be wise to send two or three missions of this type to a region prior to landing a more expensive and capable lander. The best of the scouted sites could be selected for follow-up work, and would already be mapped in 3D. 🪙
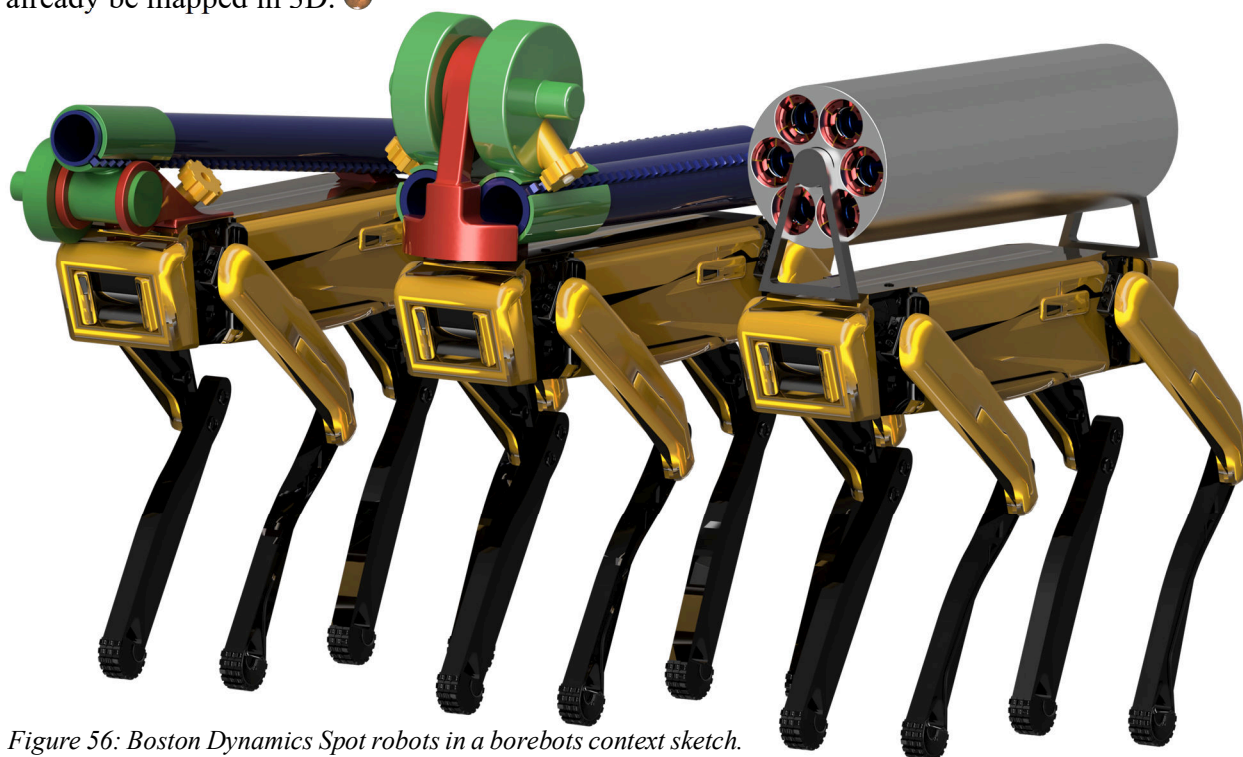

Figure 56: Boston Dynamics Spot robots in a borebots context sketch.

REFERENCES

Arthern, R. J., Winebrenner, D. P., & Waddington, E. D. (2000). Densification of Water Ice Deposits on the Residual North Polar Cap of Mars. *Icarus*, *144*(2), 367–381. https://doi.org/10.1006/icar.1999.6308

Aubrey, Andrew D., et. al. (2008). The Urey Instrument: An Advanced *In-Situ* Organic and Oxidant Detector for Mars Exploration. *Astrobiology 8*. doi:10.1089/ast.2007.0169

Balaram, J., Aung, M. & Golombek, M.P. (2021). The Ingenuity Helicopter on the Perseverance Rover. *Space Sci Rev, 217*:56. https://doi.org/10.1007/s11214-021-00815-w

Balaram, J. et al. (2018). Mars Helicopter Technology Demonstrator. *2018 AIAA Atmospheric Flight Mechanics Conference*. https://doi.org/10.2514/6.2018-0023

Bar-Cohen, Y., & Zacny, K. (Eds.). (2009). *Drilling in Extreme Environments*. Wiley. https://doi.org/10.1002/9783527626625

Bickel, B., et al. (2010). Design and Fabrication of Materials with Desired Deformation Behavior. *ACM Transactions on Graphics*, *29*(4), 1–10. https://doi.org/10.1145/1778765.1778800

Bierson, C. J., Tulaczyk, S., Courville, S. W., & Putzig, N. E. (2021). Strong MARSIS Radar Reflections From the Base of Martian South Polar Cap May Be Due to Conductive Ice or Minerals. *Geophysical Research Letters*, *48*(13). https://doi.org/10.1029/2021GL093880

Buhler, P. (2021). Personal Communication.

Byrne, S. (2009). The Polar Deposits of Mars. In *Annual Review of Earth and Planetary Sciences* (Vol. 37, pp. 535–560). https://doi.org/10.1146/annurev.earth.031208.100101

Calvin, W. (2010). *Planetary Science Decadal Survey Mars Polar Climate Concepts*. https://ia600300.us.archive.org/15/items/MarsPolarClimateConcepts/13_Mars-Polar-Climate-Final.pdf

Cappucci, S, Moulton, J., & Hengeveld, D. (2018). Assessment of the Mars Helicopter Thermal Design Sensitivities Using the Veritrek Software. *Thermal & Fluids Analysis Workshop.*

Clifford, S. M., et al. (2000). The State and Future of Mars Polar Science and Exploration. *Icarus*, *144*(2), 210–242. https://doi.org/10.1006/icar.1999.6290

Clifford, S. M., et al. (2013). Introduction to the fifth Mars Polar Science special issue: Key questions, needed observations, and recommended investigations. In *Icarus* (Vol. 225, Issue 2, pp. 864–868). https://doi.org/10.1016/j.icarus.2013.04.005

Darcy, E. & Scharf, S. (2015). "Safe, High Performing Li-ion Battery Designs: Summary of 2015 Findings." NASA Johnson Space Center. https://www.nasa.gov/sites/default/files/atoms/files/darcy_-_nasa_batt_workshop_2015.pdf

Davis, J. (2018). *PDD Completes Second Field Test*. The Planetary Society.
    https://www.planetary.org/articles/pdd-completes-second-field-test

Eshelman, E. J., et al. (2019). WATSON: In Situ Organic Detection in Subsurface Ice Using
    Deep-UV Fluorescence Spectroscopy. *Astrobiology*, *19*(6), 771–784.
    https://doi.org/10.1089/ast.2018.1925

Farley, K. A., et al. Mars 2020 Mission Overview. In *Space Science Reviews* (Vol. 216, Issue 8).
    Springer Science and Business Media B.V. https://doi.org/10.1007/s11214-020-00762-y

Garcia, I. (2013). *Sneakers with Filaflex*.
    http://web.archive.org/web/20131203233344/http://recreus.com/?p=1

Garcia, I. (2014). *Recreus sneakers II*. https://www.thingiverse.com/thing:285404

Goesmann, Fred, et. al. 2017. "Mars Organic Molecule Analyzer (MOMA) Instrument."
    Astrobiology 17, 6-7. https://doi.org/10.1089/ast.2016.1551

Great, D. (n.d.). *Boston Dynamics Spot*. Sketchfab.Com. Retrieved October 29, 2021, from
    https://skfb.ly/ooLTs

Head, J. W., & Pratt, S. (2001). Extensive hesperian-aged south polar ice sheet on Mars:
    Evidence for massive melting and retreat, and lateral flow and ponding of meltwater.
    Journal of Geophysical Research E: Planets, *106*(6), 12229–12275.
    https://doi.org/10.1029/2000je001359

Hermann, S. (2018). *Infill Pattern and Shells - How to get the Maximum Strength out of your 3D
    Prints*. https://www.youtube.com/watch?v=AmEaNAwFSfI

Hodgson, G. (Ed.). (2012). *A History of RepRap Development*.
    https://reprap.org/mediawiki/images/a/a5/A_History_of_RepRap_Development.pdf

Ion, A., Frohnhofen, J., Wall, L., Kovacs, R., Alistar, M., Lindsay, J., Lopes, P., Chen, H. T., &
    Baudisch, P. (2016). Metamaterial mechanisms. *UIST 2016 - Proceedings of the 29th
    Annual Symposium on User Interface Software and Technology*, 529–539.
    https://doi.org/10.1145/2984511.2984540

Jet Propulsion Laboratory. (2021). *NASA InSight's 'Mole' Ends Its Journey on Mars*.
    https://www.jpl.nasa.gov/news/nasa-insights-mole-ends-its-journey-on-mars

Joshi, D.R., Eustes, A. W., Rostami, J., & Dreyer, C. (2021). Evaluating Data-Driven
    Techniques to Optimize Drilling on the Moon. *SPE/IADC International Drilling
    Conference and Exhibition*. https://doi.org/10.2118/204108-MS

Kaplan, Matt, et. al. (2018). "Diving into that Lake on Mars."
    https://www.planetary.org/planetary-radio/0801-2018-garvin-mckay-mars-lake

Kerr, J. (2016). *Print-in-Place Iris Box (remix)*. Thingiverse.
    https://www.thingiverse.com/thing:1817180

Lalich, D. E., Hayes, A. G., & Poggiali, V. (2021). Explaining Bright Radar Reflections in the Martian SPLD without Liquid Water. *LPSC 2021*. https://www.hou.usra.edu/meetings/lpsc2021/pdf/2392.pdf

Lalish, E. (2013). *Gear Bearing*. Thingiverse. https://www.thingiverse.com/thing:53451

Lalish, E. (2016). *Preassembled Iris Box*. Thingiverse. https://www.thingiverse.com/thing:1811143

Lauro, S. E., et al. (2021). Multiple subglacial water bodies below the south pole of Mars unveiled by new MARSIS data. *Nature Astronomy*, *5*(1), 63–70. https://doi.org/10.1038/s41550-020-1200-6

Lauro, S. E., et al. (2019). Liquid water detection under the South Polar Layered Deposits of Mars-A probabilistic inversion approach. *Remote Sensing*, *11*(20). https://doi.org/10.3390/rs11202445

Li, J., Andrews-Hanna, J. C., Sun, Y., Phillips, R. J., Plaut, J. J., & Zuber, M. T. (2012). Density variations within the south polar layered deposits of Mars. *Journal of Geophysical Research E: Planets*, *117*(4). https://doi.org/10.1029/2011JE003937

Lockheed Martin. (n.d.). *Returning to the Red Planet*. Retrieved August 24, 2021, from https://www.lockheedmartin.com/en-us/news/features/2018/returning-to-mars.html

Magnani, P.G. et al. (2004). Deep Drill (DeeDri) for Mars Application. *Planetary and Space Science 52:*1–3, January–March 2004. doi:10.1016/j.pss.2003.08.023

Malaska, M. J., et al. (2020). Subsurface in Situ Detection of Microbes and Diverse Organic Matter Hotspots in the Greenland Ice Sheet. *Astrobiology*, *20*(10), 1185–1211. https://doi.org/10.1089/ast.2020.2241

Manning, C. V., Bierson, C., Putzig, N. E., & McKay, C. P. (2019). The formation and stability of buried polar CO_2 deposits on Mars. *Icarus*, *317*, 509–517. https://doi.org/10.1016/j.icarus.2018.07.021

Matthews, H. (2005). *Line Shaft Pulleys and Belting: Power Transmission by Belt*. Harry's Old Engine. https://www.old-engine.com/belts2.htm

Maurice, S., et al. (2021). The SuperCam Instrument Suite on the Mars 2020 Rover: Science Objectives and Mast-Unit Description. In *Space Science Reviews* (Vol. 217, Issue 3). Springer Science and Business Media B.V. https://doi.org/10.1007/s11214-021-00807-w

McKay, C. P., & Stoker, C. R. (1989). The early environment and its evolution on Mars: Implication for life. *Reviews of Geophysics*, *27*(2), 189. https://doi.org/10.1029/RG027i002p00189

Moeller, R. C., et al. (2021). The Sampling and Caching Subsystem (SCS) for the Scientific Exploration of Jezero Crater by the Mars 2020 Perseverance Rover. In *Space Science Reviews* (Vol. 217, Issue 1). Springer Science and Business Media B.V. https://doi.org/10.1007/s11214-020-00783-7

Morley, Q. (2019). *ARD3 Drive System*. Thingiverse. https://www.thingiverse.com/thing:3610134

Morley, Q. (2021). *Spherical Iris Core Catcher*. Thingiverse. https://www.thingiverse.com/thing:4864404

NASA. (2008). *Spirit Digs a Trench*. https://www.nasa.gov/multimedia/imagegallery/image_feature_133.html

NASA Mars Exploration Rovers. (n.d.). *Instruments*. Retrieved August 25, 2021, from https://mars.nasa.gov/mer/mission/instruments/

National Academies. (2003). *Assessment of Mars Science and Mission Priorities*. National Academies Press. https://doi.org/10.17226/10715

Novak, K. S., Kempenaar, J. G., Redmond, M., Daimaru, T., & Lee, C.-J. (2019). *Thermal Design of the Sample Handling Assembly in the Sampling and Caching Subsystem on the Mars 2020 Rover*. https://hdl.handle.net/2346/84712

Orosei, R., et al. (2018a). Radar evidence of subglacial liquid water on Mars. *Science*, *361*(6401). https://doi.org/10.1126/science.aar7268

Orosei, R., et al. (2018b). Radar evidence of subglacial liquid water on Mars (Supplement). *Science*, *361*(6401), 490–493. https://www.sciencemag.org/lookup/doi/10.1126/science.aar7268

Orosei, R., et al. (2018c). Radar evidence of subglacial liquid water on Mars (eLetters & responses). *Science*, *361*(6401), 490–493. https://www.sciencemag.org/lookup/doi/10.1126/science.aar7268

Phillips, R. J., et al. (2011). Massive CO2 ice deposits sequestered in the south polar layered deposits of Mars. *Science*, *332*(6031), 838–841. https://doi.org/10.1126/science.1203091

Putzig, N. E., et al. (2011). *SHARAD observations of recent geologic features on Mars (ESPC-DPS 2011)* (Issue 2). https://ui.adsabs.harvard.edu/abs/2011epsc.conf.1591P/abstract

Sanladerer, T., & Hermann, S. (2019). Silent Stepper Drivers & Topology Optimization. In *The Meltzone Podcast (46.49-56.59)*. https://www.youtube.com/watch?v=3oJBmRfcD8U

Schaler, E. W. (2021). Personal Communication.

Schumacher, C., et al. (2015). Microstructures to control elasticity in 3D printing. *ACM Transactions on Graphics*, *34*(4). https://doi.org/10.1145/2766926

Sharpe, R. D., & Cork, G. G. (1995). Geology and Mining of the Miocene Fish Creek Gypsum in Imperial County, California. In M. Tabilio & D. L. Dupras (Eds.), *29th Forum on the Geology of Industrial Minerals: Proceedings. Special Publication 110* (pp. 169–180). California Department of Conservation, Division of Mines and Geology. https://ia800309.us.archive.org/34/items/29thforumongeolo110foru/29thforumongeolo110foru.pdf

Sleater, R. (n.d.). *NASA BRAILLE: Biologic and Resource Analog Investigations in Low Light Environments*. Retrieved October 30, 2021, from https://nasa-braille.org/caves-creatures-the-cosmos/

Smith, H. D., & McKay, C. P. (2005). Drilling in ancient permafrost on Mars for evidence of a second genesis of life. *Planetary and Space Science*, *53*(12), 1302–1308. https://doi.org/10.1016/j.pss.2005.07.006

Smith, I. B., et al. (2020). The Holy Grail: A road map for unlocking the climate record stored within Mars' polar layered deposits. In *Planetary and Space Science* (Vol. 184). https://doi.org/10.1016/j.pss.2020.104841

Smith, I. B., et al. (2021). A Solid Interpretation of Bright Radar Reflectors Under the Mars South Polar Ice. *Geophysical Research Letters*, *48*(15). https://doi.org/10.1029/2021gl093618

Smith, P. H. (2005). The Phoenix mission to Mars. *2004 IEEE Aerospace Conference Proceedings (IEEE Cat. No. 04TH8720)*, 337–342. https://doi.org/10.1109/AERO.2004.1367617

Sori, M. M., & Bramson, A. M. (2019). Water on Mars, With a Grain of Salt: Local Heat Anomalies Are Required for Basal Melting of Ice at the South Pole Today. *Geophysical Research Letters*, *46*(3), 1222–1231. https://doi.org/10.1029/2018GL080985

Talalay, P.G. (2014). Drill heads of the deep ice electromechanical drills. In *Cold Regions Science and Technology* (Vol. 97, pp. 41–56). https://doi.org/10.1016/j.coldregions.2013.09.009

Talalay, P.G. (2016). *Mechanical Ice Drilling Technology*. Singapore: Springer Geophysics.

The Planetary Society. (n.d.). *Cost of Perseverance*. Retrieved August 17, 2021, from https://www.planetary.org/space-policy/cost-of-perseverance

The Planetary Society. (2016). *Planetary Deep Drill*. Retrieved from https://www.planetary.org/explore/projects/planetary-deep-drill/about-planetary-deep-drill.html

Ueda, H., & Kalafut, J. (1989). Experiments on the cutting process in ice. *CRREL Report*, *1989*(5). http://hdl.handle.net/11681/9067

Vasavada, A. R., et al. (2000). Surface properties of Mars' polar layered deposits and polar landing sites. *Journal of Geophysical Research: Planets*, *105*(E3), 6961–6969. https://doi.org/10.1029/1999JE001108

Walker, W.Q., et. al. (2017). *Statistical Characterization of 18650-format Lithium-Ion Cell Thermal Runaway Energy Distributions*. NASA Johnson Space Center.

Whitten, J. L., & Campbell, B. A. (2018). Lateral Continuity of Layering in the Mars South Polar Layered Deposits From SHARAD Sounding Data. *Journal of Geophysical Research: Planets*, *123*(6), 1541–1554. https://doi.org/10.1029/2018JE005578

Whitten, J. L., Campbell, B. A., & Plaut, J. J. (2020). The Ice Content of the Dorsa Argentea Formation From Radar Sounder Data. *Geophysical Research Letters*, *47*(23). https://doi.org/10.1029/2020GL090705

Zacny, K. (2018). *Drilling: How do we access subsurface on Mars.*

https://www.kiss.caltech.edu/workshops/marsX/presentations/Zacny.pdf

Zacny, K., et al. (2019). Application of Pneumatics in Delivering Samples to Instruments on Planetary Missions. *2019 IEEE Aerospace Conference*, 1–13. https://doi.org/10.1109/AERO.2019.8741887

Zacny, K., et al. (2016). Development of a Planetary Deep Drill. *Earth and Space 2016*, 256–266. https://doi.org/10.1061/9780784479971.027

Zacny, K., Bartlett, P., Davis, K., Glaser, D., and Gorevan, S. (2006) Test Results of Core Drilling in Simulated Ice-Bound Lunar Regolith for the Subsurface Access System of the Construction and Resource Utilization eXplorer (CRUX) Project. *Earth & Space 2006: Engineering, Construction, and Operations in Challenging Environments*. https://doi.org/10.1061/40830(188)64

Zacny, K., & Cooper, G. (2007). Methods for cuttings removal from holes drilled on Mars. *Mars 3*, 42-56. doi:10.1555/mars.2007.0004

Zacny, K., Paulsen, G., & Szczesiak, M. (2011). Challenges and Methods of Drilling on the Moon and Mars. 2011 Aerospace Conference. doi:10.1109/AERO.2011.5747261